Pulsed deformation and variable slip rates within the central Himalayan thrust belt

Delores M. Robinson[1,*] and Nadine McQuarrie[2,†]
[1]DEPARTMENT OF GEOLOGICAL SCIENCES, UNIVERSITY OF ALABAMA, TUSCALOOSA, ALABAMA 35487, USA
[2]DEPARTMENT OF GEOLOGY AND PLANETARY SCIENCES, UNIVERSITY OF PITTSBURGH, PITTSBURGH, PENNSYLVANIA 15260, USA

ABSTRACT

Forward modeling reconstructions and data derived from the Himalayan thrust belt and the foreland basin of far western Nepal tie the erosional unroofing and associated deposition to the kinematics and age of fault motion. We reproduce the deformation identified at the surface through a forward-propagating, linked fold-and-thrust belt–foreland basin system. This approach permits estimates of the magnitude of erosion at each time step and the extent, depth, and age of the associated foreland basin. The model reconstructions reveal that the units that supplied the sediment to the foreland basin changed through time: 25–13 Ma, erosion of the Tethyan Himalaya; ca. 12 Ma, first exposure of the Greater Himalaya; ca. 11 Ma, first exposure of the Lesser Himalaya. In our model, exposure of Greater Himalaya and Lesser Himalaya rock is associated with the formation of a thrust ramp that cuts through 7 km of footwall Lesser Himalaya stratigraphy and translates >7 km of Lesser Himalaya rock over the ramp, forming a Lesser Himalaya duplex. An increase in structural relief focuses erosion over the region of the ramp and facilitates exposure of Greater Himalaya and Proterozoic Lesser Himalaya rocks. As the Lesser Himalaya ramp propagates southward, more Lesser Himalaya thrust sheets are incorporated into the Lesser Himalaya duplex. Although uniquely dating thrust events is challenging, these model reconstructions allow us to associate time steps with an age of deposition or exhumation. What emerges is a tempo of deformation that varies with time, marked by periods of rapid shortening during propagation of the Main Central thrust, Ramgarh thrust, and middle stages of the development of the Lesser Himalaya duplex (~25–30 mm/yr). After emplacement of the Ramgarh thrust, early and late stages of Lesser Himalaya duplex development are marked by periods of slow shortening (~13–14 mm/yr). Although long-term and modern (geodetic) rates of deformation agree at ~20 mm/yr, rates of shortening through time have varied from 4 to 33 mm/yr.

LITHOSPHERE; v. 4; no. 5; p. 449–464 | Published online 5 September 2012 doi: 10.1130/L204.1

INTRODUCTION

Fold-and-thrust belts such as the Himalaya are intrinsically linked to their frontal foreland basins. Understanding the geometry and kinematics of this paired system is a requirement for evaluating the interplay between deformation and climate and their influence on erosion and deposition (Koons, 1990; Willett et al., 1993; Burbank et al., 2003; Thiede et al., 2004; Upton et al., 2009). The Himalaya were formed as the Indian plate moved northward and collided with the Asian plate. After initial collision, deformation propagated southward and built an early fold-and-thrust belt in Neoproterozoic–Paleozoic Tibetan or Tethyan Himalaya rocks (Ratschbacher et al., 1994; Murphy and Yin, 2003) before incorporating the highly metamorphic Neoproterozoic–Ordovician Greater Himalayan rocks and the more proximal to India, Proterozoic Lesser Himalayan rocks into the growing orogen (e.g., Gansser, 1964; LeFort, 1975). This evolving system of folded and faulted rocks shed detritus into the adjacent foreland basin, which was then assimilated into the orogenic system as the Foreland Basin sequence and the Subhimalaya (Burbank et al., 1996; DeCelles et al., 1998b, 2004). The Himalayan Mountains continue to shed sediment into the modern Indo-Gangetic foreland basin.

Because the Himalaya is the largest active continent-continent collision on Earth, it is a testing ground for kinematic and dynamic models focused on understanding collisional orogens, the feedback between erosion and tectonics, and the principal drivers that partition deformation and convergence. A common approach to documenting the structural geometry of the Himalaya is through balanced cross sections (e.g., Long et al., 2011, and references therein). These cross sections illustrate a possible geometry of the thrust belt, while the restored sections are a representation of undeformed stratigraphy prior to the Himalayan collision. In these static cross sections, undeformed and deformed sections are presented without showing how the thrust belt developed kinematically. However, implied in every cross section is a kinematic sequence necessary to reproduce the illustrated deformation, which can be shown through a series of sequential reconstructions that are balanced at every step (e.g., Robinson, 2008). Although viable, these modeling reconstructions do not have absolute time assigned to the frames, and no effort is made to account for erosion of the stratigraphic overburden or flexure of the Indian plate at each step in the reconstruction. Determining the time of fault initiation and duration in order to place an absolute time frame in sequential deformation steps is difficult because the age of faulting can rarely be directly measured. However, geochronologic ages of mineral systems provide records of burial, and thermochronologic ages of mineral systems provide records of exhumation. Bracketing the interval between deposition and exhumation provides an indirect age for the initiation of motion on thrust faults. In addition, if a well-dated foreland basin can be tied to a period of time when the fold-and-thrust belt was deforming and eroding, then the foreland basin succession may be used to place age brackets on the deformation (e.g., Najman et al., 2004, 2009; van der Beek et al., 2006; Szulc et al., 2006; Ravikant et al., 2011).

Fold-and-thrust belts can be characterized to a first order by critical taper wedge theory (Chapple, 1978; Davis et al., 1983; Dahlen, 1990). The metamorphosed and penetratively strained core of the Himalayan orogen

*E-mail: dmr@geo.ua.edu.
†E-mail: nmcq@pitt.edu.

is thought by many to preclude its inclusion in a coupled thrust belt–foreland basin system or to be viewed as part of a critically tapered system (e.g., Searle et al., 2008). Although Greater Himalaya rocks have a pronounced flattening fabric (Law et al., 2004; Long and McQuarrie, 2010) and are penetratively strained (e.g., Larson et al., 2010), Greater Himalaya rock was emplaced over 125 km of Lesser Himalaya rocks along a singular structure, the Main Central thrust (Brunel, 1986; Schelling and Arita, 1991; Robinson et al., 2003, 2006). Although we recognize the ductile nature of Greater Himalaya rocks, we do not attempt to include penetrative deformation. The first-order constraint of Main Central thrust and Greater Himalaya evolution is the motion on the Main Central thrust required by the southernmost cutoffs of the Greater Himalaya rocks to emplace 125 km of Greater Himalaya over Lesser Himalaya rock. Precedence for including highly metamorphosed and strained "basement" rocks as part of fold-and-thrust belt systems exists in the Pyrenees (Sinclair et al., 2005), northern Scandinavian Caledonides (Northrup, 1996), and Appalachians (Mitra, 1978; Boyer and Elliott, 1982; Hatcher and Hooper, 1992).

The purpose of this study is to link the deformation, erosion, and depositional history of the Himalayan orogen in far western Nepal to forward models of thrust belt deformation through the incorporation of multiple data sets. We constructed a sequentially restored, structural model based on the kinematic sequence inherent in a balanced cross section using the reconstruction program 2D Move to evaluate the co-evolution of the fold-and-thrust belt and its associated foreland basin. Using 2D Move, we modeled the dimensions of a flexural foreland basin by determining the structural elevation and associated isostatic loading from thrust sheet emplacement, followed by isostatic unloading from erosion. By assuming a topographic wedge that mimics the modern increase in elevation from the Indo-Gangetic foreland to the Tibetan Plateau over ~150 km (~2° topographic slope), we can estimate the magnitude of rock eroded in each time step and the expected stratigraphy exposed in the thrust belt. Each increment of thrust emplacement deforms the topographic surface. The difference between the deformed topography and the original topography becomes a gravitational load that flexes the Indian plate, increases the angle of the basal décollement, and creates a foreland basin. The difference between the deformed topography and the new topographic ramp from the deformation front to the hinterland defines the amount of material removed by erosion. Although this approach does not account for topographic details, we show that this first-order approximation allows us to predict depths to thermochronologic and geochronologic samples that can be compared with closure temperatures and ages as well as predicting the age, detrital input, and location of an evolving foreland basin. We compare the burial, exhumational, and depositional history of our sequential reconstruction to published geochronologic and thermochronologic data from the hinterland, as well as detrital zircon U-Pb ages, epsilon Nd values, trace-element data, bulk petrography, sedimentology, and magnetostratigraphic data from the foreland basin. This approach documents the tempo of both deformation and exhumation in the Himalayan thrust belt of far western Nepal from 25 Ma to the present, even within the uncertainty inherent in the evolution of topography with time.

STRATIGRAPHY, KINEMATICS, AND KNOWN TIMING HISTORY

Nepal is located in the central part of the Himalayan arc, which extends ~2400 km between the eastern to western syntaxes (Fig. 1A). Far western Nepal is situated in the apex of the Himalayan arc and is the location of

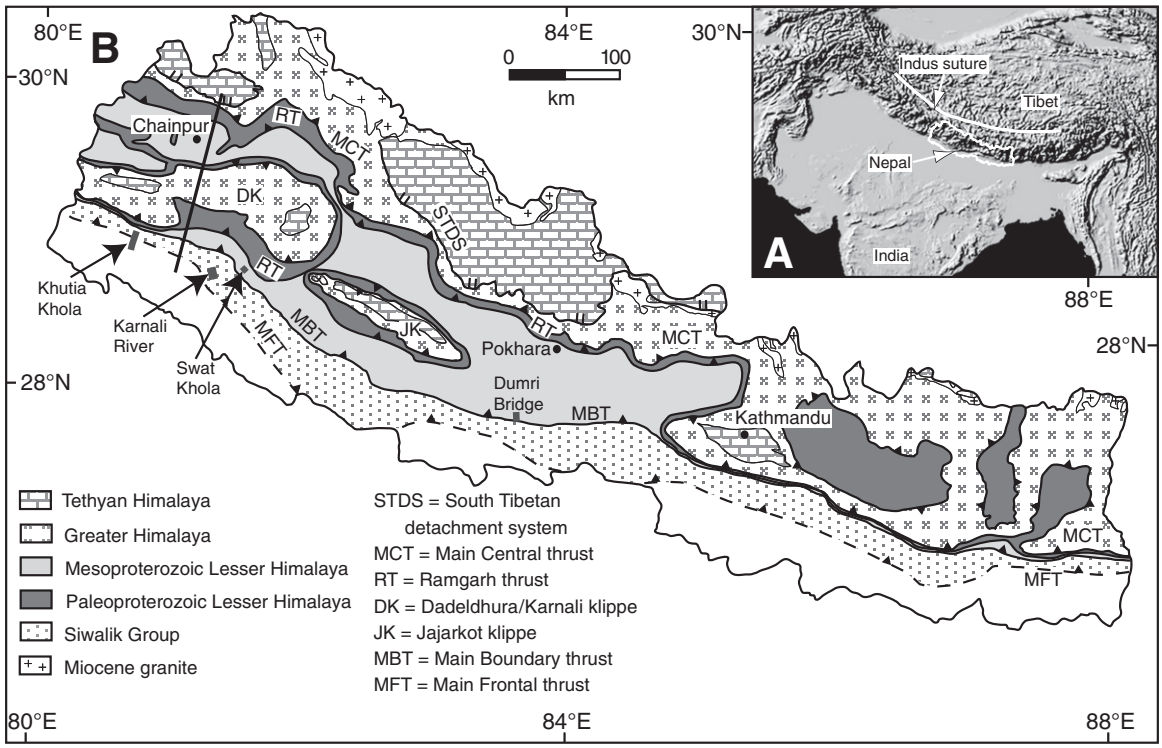

Figure 1. (A) Digital image of the Himalayan-Tibetan orogenic system from the Global 30 Arc-Second Elevation Data Set. Nepal is outlined in white for reference. (B) Geologic map of Nepal modified from Robinson and Pearson (2006) and loosely based on Amatya and Jnawal (1994). Dark-gray boxes indicate locations of foreland basin data referred to in text. The location of the reconstruction line is shown with a black line. Foreland basin data locations are marked with short gray lines. Thrust faults are indicated with barbs. Normal faults are indicated with two parallel lines. Cities are indicated with a solid black circle.

the largest magnitude of horizontal shortening estimated in the Himalaya (Robinson et al., 2006; see review in Long et al., 2011).

The Tibetan part of the Himalayan thrust belt system consists of the high peaks of the Himalaya northward to the Indus suture and contains Tethyan Himalaya rocks (Fig. 1B). Most researchers agree that deformation began at the initiation of the collision of India with Asia at ca. 50–55 Ma (Zhu et al., 2005; Najman, 2006; Green et al., 2008; Dupont-Nivet et al., 2010; Najman et al., 2010; Wang et al., 2011) and continued deforming and shortening Tethyan Himalaya rocks until 30–25 Ma (Fig. 2; e.g., Ratschbacher et al., 1994; Webb et al., 2011). As the Tibetan thrust belt thickened and deformed Tethyan Himalaya rocks, Greater Himalaya rocks underneath the thrust belt were buried, metamorphosed, and transported southward via a shear zone, the Main Central thrust (LeFort, 1986; Vannay and Hodges, 1996; Catlos et al., 2001; Daniel et al., 2003). As this fault advanced above the brittle-ductile transition zone, it evolved into a more brittle fault, as found in the synformal klippen in Nepal (Fig. 1B). In far western Nepal, $^{40}Ar/^{39}Ar$ cooling ages on muscovite suggest that the Main Central thrust was active at ca. 25–21 Ma (Fig. 2; DeCelles et al., 2001; Robinson et al., 2006). Greater Himalaya rocks consist of a 5–20-km-thick assemblage of Late Proterozoic–early Paleozoic metamorphic rock (LeFort, 1975; Parrish and Hodges, 1996; DeCelles et al., 2000; Gehrels et al., 2003; Martin et al., 2005).

Emplacement of the Greater Himalaya rock on top of the cooler Lesser Himalaya rock along the Main Central thrust initiated burial and metamorphism of Lesser Himalaya strata (e.g., Hodges, 2000). In western and central Nepal, Lesser Himalaya rocks contain three superimposed rock sequences, the Lesser Himalayan sequence, the Gondwana sequence, and the Foreland Basin sequence. Detrital zircon data indicate that the Lesser Himalaya sequence was derived from the Indian craton in Paleoproterozoic to Mesoproterozoic time (e.g., DeCelles et al., 2000; Gehrels et al., 2011, and references therein). This study divides the Lesser Himalaya sequence into the Paleoproterozoic Lesser Himalaya rock, containing Kushma and Ranimata Formations and the ca. 1.73–1.86 Ga Proterozoic augen gneiss (dark gray, Fig. 1B), and the Mesoproterozoic Lesser Himalaya rock, containing the Sangram, Galyang, and Syangia Formations and the Lakharpata Group (light gray, Fig. 1B; Upreti, 1996, 1999; DeCelles et al., 2001; Robinson et al., 2006; Martin et al., 2011). In central Nepal, the Mesoproterozoic Lesser Himalaya units are overlain by the late Paleozoic and Mesozoic Gondwana sequence (Sakai, 1983, 1989). In far western Nepal, a thin unit similar to the Gondwana sequence is poorly exposed and intensely deformed (Robinson et al., 2006). The Foreland Basin sequence is composed of synorogenic sediment shed from the Himalayan thrust belt beginning in mid- to late Eocene time (Sakai, 1983) and consists of the Bhainskati Formation and the Dumri Formation (Sakai, 1983; DeCelles et al., 1998b). In western Nepal, the Dumri and Bhainskati Formations are found north of the Main Boundary thrust and are incorporated into the thrust belt (Robinson et al., 2006). The youngest synorogenic sediment is placed into a different tectonostratigraphic zone, the Subhimalaya, which is a 10–30-km-wide belt of imbricated Neogene Siwalik Group strata (Burbank et al., 1996) located exclusively south of the Main Boundary thrust at the toe of the thrust belt.

Major faults and structures south of the Main Central thrust in far western Nepal include the Ramgarh (Munsiari) thrust, Lesser Himalayan duplex, Dadeldhura thrust, Lesser Himalayan imbricate zone, Main Boundary thrust, and Main Frontal thrust (Figs. 1B, 2, and 3). The Ramgarh thrust is exposed in the footwall of the Main Central thrust, conformably underlies the Dadeldhura klippe in the north and south, and displaces Paleoproterozoic Lesser Himalaya rock >120 km to the south (Robinson et al., 2006). The Dadeldhura klippe (Fig. 1B), underlain by the Dadeldhura thrust, is part of the Lesser Himalaya "crystalline klippe."

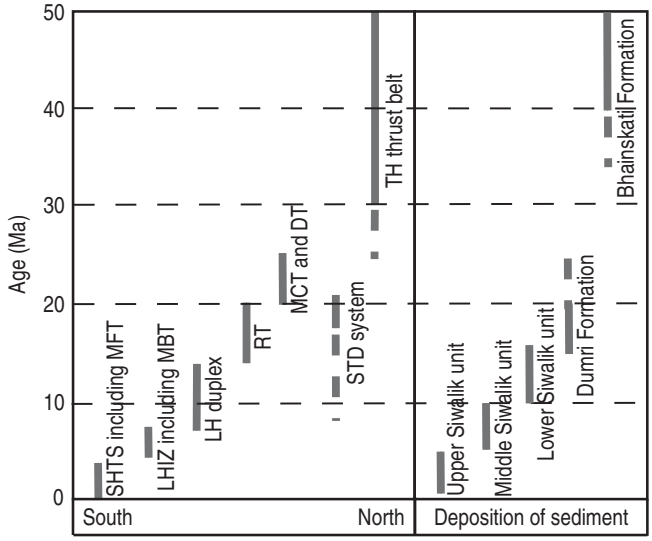

Figure 2. Left side: Timing of motion of faults in far western Nepal. Right side: Timing of deposition of sediment in the Siwalik Group and Foreland Basin sequence. All data plus references are in the text. Timing is indicated by the solid gray line. The dashed line indicates that the timing may extend farther. Abbreviations are: TH—Tethyan Himalaya, STD—South Tibetan detachment, MCT—Main Central thrust, DT—Dadeldhura thrust, RT—Ramgarh thrust, LH duplex—Lesser Himalayan duplex, LHIZ—Lesser Himalayan imbricate zone, MBT—Main Boundary thrust, SHTS—Subhimalayan thrust system, MFT—Main Frontal thrust.

These synformal klippen have Greater Himalaya affinity (e.g., Robinson et al., 2001) and are interpreted to have been emplaced via motion on the Main Central thrust (Johnson et al., 2001; Johnson, 2005; Pearson and DeCelles, 2005), which in turn was passively carried by the Ramgarh thrust. The Lesser Himalaya duplex is a hinterland-dipping antiformal duplex between the Main Central thrust and Dadeldhura thrust. These thrust sheets were once continuous but became erosionally separated via the development of the Lesser Himalaya duplex, which folded the overlying Greater Himalaya rock into broad antiformal (over the duplex) and synformal (in front of the duplex) structures (Fig. 3) (Robinson et al., 2001, 2003). Erosion through Greater Himalaya rocks stranded the "crystalline klippe" and cast uncertainty on the relationship between the Dadeldhura thrust and the Main Central thrust to the north. South of the Dadeldhura klippe, there is a sequence of complexly deformed Lesser Himalaya rock in the frontal part of the thrust belt called the Lesser Himalaya imbricate zone, of which the southernmost fault is the Main Boundary thrust, active as late as 4–5 Ma (DeCelles et al., 1998b) (Fig. 3). South of the Main Boundary thrust, synorogenic Siwalik Group strata are deformed by the Subhimalayan thrust system (Fig. 3). These Subhimalaya imbricated panels are separated from the Quaternary to modern sediments of the Indo-Gangetic plain by the active Main Frontal thrust (e.g., Lavé and Avouac, 2000). All faults are assumed to sole into the main décollement at the base of the thrust belt, the Main Himalayan thrust.

DEPOSITIONAL AGE, PROVENANCE, AND SEDIMENTOLOGICAL CHARACTERISTICS OF FORELAND BASIN ROCKS

Pre–Foreland Basin Rocks

In late Paleozoic to Mesozoic time, the Gondwana sequence was deposited unconformably on top of the Proterozoic Lesser Himalaya

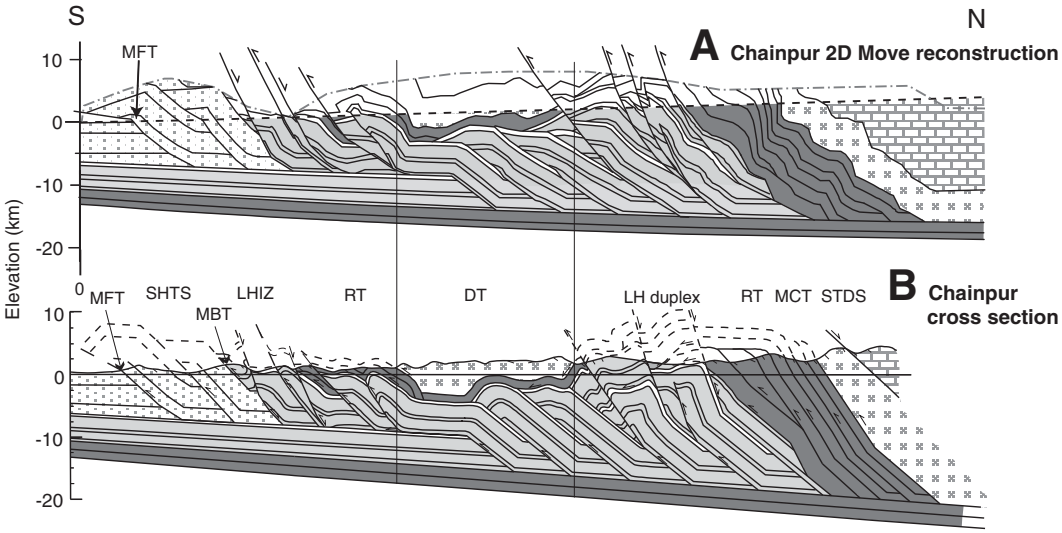

Figure 3. (A) The final cross section derived from the reconstruction program shown in Figure 4H. (B) The final balanced cross section from Robinson et al. (2006). The cross sections are aligned by vertical lines to the north and south of the Dadeldhura klippe for comparison. Abbreviations and patterns are the same as Figure 1B and 2, except that in these cross sections, the Dumri Formation is solid white instead of grouped in with the light-gray Mesoproterozoic stratigraphy.

sequence. Detrital zircon U-Pb ages from the Charchare conglomerate, a unit in the lower part of the Gondwana sequence, indicate a maximum depositional age of 125 ± 1 Ma (DeCelles et al., 2004) (Table 1). The overlying Amile Formation was deposited between Early Cretaceous to possibly early Eocene time (Sakai, 1983). Table 1 shows detrital zircon U-Pb age populations that indicate the sedimentary source was the Early Proterozoic to Archean rocks of the northern Indian craton located to the south (DeCelles et al., 2000, 2004).

Bhainskati Formation

Deposition of the Bhainskati Formation marks the beginning of the Foreland Basin sequence (Fig. 2) (DeCelles et al., 2004). In far western Nepal, the thickness of the Bhainskati Formation is estimated at ~100 m. The suggested age for the lower portion of the formation is late Paleocene–early Eocene (Fuchs and Frank, 1970), and the upper portion has a mid–late Eocene age based on foraminifera and marine fossils (Sakai, 1983). Najman et al. (2005) records a 45 Ma zircon population in the upper half of the Bhainskati Formation in central Nepal at Dumri Bridge (Fig. 1B), requiring that the upper half be younger than 45 Ma.

Table 1 shows the detrital zircon U-Pb age populations present in the Bhainskati Formation. These age groups are found in both Tethyan Himalaya and Greater Himalaya rocks and indicate a Himalayan thrust belt source. The average $\varepsilon_{Nd(T)}$ value is −10 for the Bhainskati Formation (DeCelles et al., 2004), which is less negative than the average $\varepsilon_{Nd(T)}$ value of Greater Himalaya rocks (−16; Robinson et al., 2001), suggesting either a Tethyan Himalaya source, or an additional component of less-evolved detritus. In the correlative Subathu Formation (NW India), the lower half of the formation is more enriched in Ni and Cr, and is interpreted as originating in the mafic arc and ophiolitic rocks of the Indus suture (Najman

TABLE 1. DATA FROM THE FORELAND BASIN SEDIMENTS

Unit	Age	Detrital zircon U-Pb age groups (Ma)	Mean ε_{Nd}	Other	Bulk petrography	Provenance
Bhainskati Formation	Early–mid-Eocene[1,2,4]	ca. 500–800 ca. 1000–2100 ca. 2400–3200[6]	−10[6]	Lower half has high Cr and Ni; upper half has low Cr and Ni[4,10]	Monocrystalline[5]	TH source[6]
Oxisol—Late Eocene–Oligocene 40 or 35 Ma to ca. 20 Ma (15–20 m.y.)[5]						
Dumri Formation	Early Miocene 19.9–15.1 Ma[4,6,9]	Same as Bhainskati; increase in ca. 1000–1500 and 470–500 grains[6]	−14.4[6,12]	Low Cr and Ni[4,10]	Decrease in quartz; increase in lithics; low-grade metasedimentary lithic fragments; increase in plagioclase[5]	Ambiguous source TH or GH
Lower Siwalik unit	Middle Miocene >13.3 to ca. 10 Ma[8,9]	Same as Dumri; increase in ca. 1000–1500 and 470–500 grains[6]	−16[11,12]		First appearance of kyanite and sillimanite lithic fragments at ca. 11 Ma[5]; coarsening grain size at micro- and macroscale[7,11]	TH and unambiguous GH source at ca. 11 Ma
Middle Siwalik unit	ca. 10.5 to ca. 4.6 Ma[3,5,7,8,9]	Same as lower Siwalik; increase in ca. 1800 grains[6]	−18[11,12]	First appearance of LH-derived carbonate clasts[5]	No data	Continued TH/GH source; new LH source
Upper Siwalik unit	>4.6 Ma[3,5,7,8,9]	Same as middle Siwalik[6]	−18[11,12]	Proximal LH clasts[5]	No data	Continued TH/GH and LH source

Note: References: 1—Fuchs and Frank (1970); 2—Sakai (1983); 3—Quade et al. (1995); 4—Najman et al. (1997, 2005); 5—DeCelles et al. (1998a, 1998b); 6—DeCelles et al. (2000, 2001, 2004); 7—Nakayama and Ulak (1999); 8—Gautam and Fujiwara (2000); 9—Ojha et al. (2000, 2009); 10—Najman and Garzanti (2000); 11—Huyghe et al. (2001, 2005); 12—Robinson et al. (2001). Abbreviations: Cr—chromium; Ni—nickel; TH—Tibetan Himalaya; GH—Greater Himalaya; LH—Lesser Himalaya.

and Garzanti, 2000; Najman et al., 2005). The upper half of the formation has lower concentrations of Ni and Cr, which may indicate a shift in the source material to sedimentary rocks of the Tethyan Himalaya (Najman and Garzanti, 2000; Najman et al., 2005).

The base of the formation has phosphatic and organic-rich mud rock and limestone that transitions up stratigraphic section into oolitic ironstone, suggesting that paleobathymetry gradually shoaled until the depositional site lay above wave base but far enough offshore to prevent the influx of siliciclastic detritus (DeCelles et al., 1998b). On top, a well-developed unconformity, a paleosol, spans late Eocene–Oligocene time, and has been interpreted to represent subaerial exposure until ca. 20 Ma (DeCelles et al., 1998b). This paleosol is present at Dumri Bridge but absent at Swat Khola (Fig. 1B), which led DeCelles et al. (1998b) to speculate that the paleosol was erosionally removed before deposition of the Dumri Formation. Using the definitions of DeCelles and Giles (1996), the Bhainskati Formation is interpreted as a back-bulge depozone, with the condensed section indicating the southward migration of the forebulge, and deposition of the overlying Dumri Formation marking the beginning of distal foredeep deposition (DeCelles et al., 1998b).

Dumri Formation

At Dumri Bridge (Fig. 1B) in south-central Nepal, the contact is sharp between the Bhainskati paleosol and the red rocks of the 800–1200-km-thick Dumri Formation (DeCelles et al., 1998b). Here, the youngest zircon population shows that the base is younger than 30–32 Ma (Najman et al., 2005). To the north, near the town of Chainpur (Fig. 1B), the lower half of the formation is a green, strongly indurated, micaceous sandstone. Approximately 30 m up section, a pronounced bauxite paleosol occurs with kaolinite and hematite pisolites, above which the formation returns to a micaceous sandstone. The upper half of the formation is dominated by red and green shale. Detrital micas provide a $^{40}Ar/^{39}Ar$ age from the lower micaceous sandy section of ca. 20 Ma (SR9), the maximum age of the Dumri Formation in this location (DeCelles et al., 2001). Additional Dumri Formation conglomerate crops out north of this sample, suggesting that there, the formation could be older. In the south, near the Main Boundary thrust, Ojha et al. (2009) suggested an age at Swat Khola of 19.9–15.1 Ma using magnetostratigraphy.

Table 1 shows the detrital zircon U-Pb age populations, which are similar to that of the Bhainskati Formation, except more grains in the 470–500 Ma and ca. 1000–1500 Ma age ranges (DeCelles et al., 2004). Because the detrital zircon age spectra for the Greater Himalaya and Tethyan Himalaya rocks are so similar (e.g., Amidon et al., 2005), they cannot be used to identify when Greater Himalaya rocks began to supply detritus. The average $\varepsilon_{Nd(T)}$ value is −14.4 (Robinson et al., 2001), indicating that the formation is more isotopically evolved than Bhainskati Formation. This value is similar to both Tethyan Himalaya and Greater Himalaya average values (Robinson et al., 2001).

Correlative strata in NW India show low Cr and Ni, compatible with a Tethyan Himalaya or Greater Himalaya source (Najman and Garzanti, 2000; Najman et al., 2005). Petrographic studies reveal abundant low-grade metasedimentary lithic grains, indicating the first evidence of eroded metamorphic rocks. DeCelles et al. (1998b) documented significant amounts of plagioclase, which they interpreted as originating from Greater Himalaya affinity rocks from the Dadeldhura klippe (Fig. 1B). To the east of the Dadeldhura klippe, in west-central Nepal (Fig. 1B), Sakai et al. (1999) noted the lack of high-grade metamorphic lithic fragments, and suggested that the phyllitic lithic fragments were supplied from lower Lesser Himalaya and/or Tethyan Himalaya rock. Sakai et al. (1999) also reported a $^{40}Ar/^{39}Ar$ muscovite cooling age of 16–17 Ma, which they interpreted as cooling from emplacement of the Main Central thrust over these foreland basin rocks.

Siwalik Group

The Siwalik Group is a middle Miocene to Pliocene belt of synorogenic foreland basin sediment at the front of the thrust belt informally divided into upper, middle, and lower units (Fig. 2; Quade et al., 1995). This division is predominantly lithostratigraphic, and so it is useful for broad regional comparisons but cannot be used for detailed chronostratigraphy (DeCelles et al., 1998a). The cross section from which the reconstruction is derived for this study is located along the straight black line in Figure 1B. In the Subhimalaya, this line falls in between two measured sections though the Siwalik Group at Khutia Khola and Karnali River (thick gray lines, Fig. 1B).

Lower Siwalik Unit

At Khutia Khola, deposition of the lower Siwalik unit began by ca. 13.3 Ma (Ojha et al., 2000); however, the base is covered by alluvium, so the unit may be as old as 15.1 Ma, the youngest Dumri Formation rock. The thickness is 862 m of interbedded sandstone and shale (DeCelles et al., 1998a). At the Karnali River, deposition began at 16 Ma, and the thickness of the unit is ~2000 m (Gautam and Fujiwara, 2000). Detrital zircon U-Pb ages (Table 1) show the same zircon ages as found in the Dumri Formation, in addition to an increase in grains from the ~1000–1500 Ma and 470–500 Ma populations (DeCelles et al., 2004). The average $\varepsilon_{Nd(T)}$ value is −16, the same as the average for Greater Himalaya and Tethyan Himalaya rocks (Huyghe et al., 2001; Robinson et al., 2001). The first appearance of high-grade metasedimentary lithic grains, kyanite and sillimanite, occurs in the upper part of the lower Siwalik unit at Khutia Khola (DeCelles et al., 1998b), which is dated at ca. 11 Ma (Ojha et al., 2000). Thus, Greater Himalaya rocks were at the surface contributing sediment at this time. At 10–11 Ma at the Karnali River, Huyghe et al. (2001) noted a coarsening grain size at the microscopic scale, and Nakayama and Ulak (1999) noted a similar coarsening at the macroscopic scale.

Middle Siwalik Unit

As noted already, the reconstruction we present here is in between the physical locations of Khutia Khola, where the lithologic change from lower to middle Siwalik units is at 10.8 Ma (Ojha et al., 2000), and the Karnali River, where the lower to middle transition is at 9.7 Ma (Gautam and Fujiwara, 2000). Between 11 and 9.7 Ma, a distinct normal polarity chron (5n) can be identified on both paleomagnetic data sets and tied to the geomagnetic polarity time scale (Cande and Kent, 1995). In Khutia Khola, this chron is within the middle Siwalik unit; however, in the Karnali River section, this chron is within the lower Siwalik unit. Because the change in lithology that defines the boundary between the lower and middle Siwalik units occurs at different times in these two sections, we tie our observations to both lithology and age. Table 1 combines both sections and groups data older than 10 Ma in the lower Siwalik unit and younger than 10 Ma in the middle Siwalik unit.

The thickness of the middle Siwalik unit at Khutia Khola is 2468 m and is dominated by stacked channel sandstones punctuated by thin shale beds (DeCelles et al., 1998a). Lesser Himalaya–derived carbonate clasts first appear at the base of the section (at 10.8 Ma), and the magnitude increases up section. An upward excursion in the $^{87}Sr/^{86}Sr$ ratio of pedogenic carbonate nodules in mudstone at ca. 9 Ma is another indication of Lesser Himalaya carbonate erosion (Quade et al., 1997). The carbonate clasts are derived from the Mesoproterozoic Lakharparta Group and not the Paleoproterozoic lower Lesser Himalaya rocks, indicating

derivation from rocks in the Lesser Himalaya duplex. In addition, $\varepsilon_{Nd(T)}$ values become more negative, from −16 to −18 between 10 and 9 Ma, and remain at these values throughout middle Siwalik unit deposition (Robinson et al., 2001). The transition between the lower to middle units in the Karnali River section is marked by prevalence of stacked fluvial channel sandstones. The section is ~1500 m thick; detrital staurolite first occurs at 9–10 Ma, and detrital kyanite first occurs at 8 Ma (Szulc et al., 2006). The $\varepsilon_{Nd(T)}$ values from the Karnali River section become markedly negative (−18) at 10 Ma, indicating influx of Lesser Himalaya material (Huyghe et al., 2001; Szulc et al., 2006). Most U-Pb detrital zircon studies do not break out the lower, middle, and upper Siwalik units, and instead discuss trends. In the middle and upper Siwalik units, the proportion of Lesser Himalaya rock having detrital zircon with U-Pb ages older than 2 Ga increases up stratigraphic section (DeCelles et al., 1998b), indicating the unroofing of Lesser Himalaya rocks.

Upper Siwalik Unit

The middle to upper Siwalik unit transition at Khutia Khola is estimated at younger than 4.5 Ma (Ojha et al., 2000). The thickness at Khutia Khola is at least 1000 m thick and is dominated by fluvial conglomerate punctuated by fluvial sandstone (DeCelles et al., 1998a). This unit was not measured at Karnali River (Gautam and Fujiwara, 2000), but was determined to be younger than 5 Ma. The trends of the detrital zircon age populations and $\varepsilon_{Nd(T)}$ values are similar to those of the middle Siwalik unit (Table 1). After 4–5 Ma in Khutia Khola, a proximal facies is indicated by the appearance of Lesser Himalaya conglomerate clasts (DeCelles et al., 1998b), suggesting a nearby surface exposure of Lesser Himalaya rocks.

HINTERLAND DATA

Far western Nepal is remote and difficult to access. As such, existing data sets are sparse (Table 2). DeCelles et al. (2001) reported a $^{40}Ar/^{39}Ar$ muscovite cooling age of ca. 21 Ma in the Budhiganga gneiss (SR40; DeCelles et al., 2001) from the northern limb of Dadeldhura thrust sheet in the Dadeldhura klippe. Robinson et al. (2006) reported a $^{40}Ar/^{39}Ar$ muscovite cooling age of ca. 25 Ma in the hanging wall of the Main Central thrust sheet (SR124). These two ages are in Greater Himalaya rocks (Table 2) and are located along the reconstruction line. East of the Karnali River (Fig. 1B), Sakai et al. (1999) reported an Ar plateau age of 25.69 ± 0.13 Ma for biotite in gneiss on the southern limb of the Dadeldhura klippe in Greater Himalaya rocks. These ages indicate that in far western Nepal, Greater Himalaya rocks cooled through the blocking temperature for muscovite and biotite from 25 to 21 Ma, and these are interpreted to represent cooling due to erosional exhumation that accompanied initial motion along the Main Central thrust (Fig. 2).

In far western Nepal, the northernmost exposure of Lesser Himalaya rocks in the Lesser Himalaya duplex indicates peak temperatures of 500–550 °C, identified using Raman spectroscopy of carbonaceous material (Bollinger et al., 2004). Beyssac et al. (2004) reported that the Raman spectroscopy of carbonaceous material temperatures in Lesser Himalaya rock along the Nepal-India border decrease gradually from 540 °C in the footwall of the Main Central thrust to 330 °C in the middle of the Lesser Himalaya duplex. This southward decrease in temperature away from the Main Central thrust indicates that the magnitude of overburden that buried these samples also decreases to the south. In addition, the temperatures indicate that the northernmost Lesser Himalaya rocks reached the temperatures necessary to reset $^{40}Ar/^{39}Ar$ muscovite cooling ages. Robinson et al. (2006) reported a $^{40}Ar/^{39}Ar$ muscovite cooling age from the Ramgarh thrust sheet (SR123) of 17–7 Ma in far western Nepal (Table 2). A $^{40}Ar/^{39}Ar$ muscovite cooling and isochron age of 12.5–12 Ma (SR103a; Robinson et al., 2006) was also reported from the northern part of the Lesser Himalaya duplex (Table 2).

Due to the remote location, no paleobarometric data exist for far western Nepal. Thus, the only data available are via extrapolation from central Nepal, where the Ramgarh thrust experienced peak pressures of 10 kbar at a temperature of ~550 °C, and the Main Central thrust experienced peak pressures of 12 kbar at a temperature of ~725 °C (Kohn, 2008), corresponding to 35 and 42 km, assuming a buoyant crust. However, the thickness of the Greater Himalaya rocks in central Nepal (16 km) is doubled by the Langtang thrust. The distance from the Main Central thrust to the Langtang thrust is 8 km (Kohn, 2008). Along the reconstruction line in this study, Greater Himalaya thickness is 8 km and restores to a much shallower ~25 km depth, with the approximate location shown in Figure 4A.

MODEL ASSUMPTIONS AND PARAMETERS

We link the exhumation documented in the hinterland to the depositional history of the foreland basin using a sequentially restored balanced cross section. We model the sequential deformation and associated erosion and deposition, and use the published data to validate the model, which predicts the magnitude of exhumation, depositional basin extent, and the stratigraphic units that were exposed at the surface. This approach allows us to use published ages of exhumation and deposition to place age constraints on fault motion, but it requires several assumptions that are detailed in the following section.

Assumptions

Geometry of the Original Indian Margin

The initial configuration of the units before 25 Ma is portrayed as flat-lying, undeformed strata on the northern Indian margin. This configuration contains simplifications and assumptions.

(1) Pre-Himalayan deformation of Proterozoic rocks. The Lesser Himalaya rocks in far western Nepal are predominantly Proterozoic in age and may have experienced several periods of deformation. Intrusive bodies 1.73–1.86 Ga in age indicate a Himalayan-wide arc event (for more

TABLE 2. HINTERLAND DATA

Thrust sheet	Reference	Sample	Figure	Age (Ma)
DT/MCT, Budhiganga gneiss	DeCelles et al. (2001)	SR 40	4B	21.1 ± 0.2
MCT, GH	Robinson et al. (2006)	SR 124	4B	ca. 25
DT/MCT, gneiss*	Sakai et al. (1999)	n/a†	n/a	25.68 ± 0.13
RT, schist	Robinson et al. (2006)	SR 123	4C	17.8 ± 0.8 to 7.3 ± 0.5
Northern LH duplex, phyllite	Robinson et al. (2006)	SR 103a	4E	12.41 ± 0.16 to 12.01 ± 0.05

*Ar plateau age in biotite; all other ages are $^{40}Ar/^{39}Ar$ muscovite cooling ages. Abbreviations as in Figure 1.
†n/a—not available.

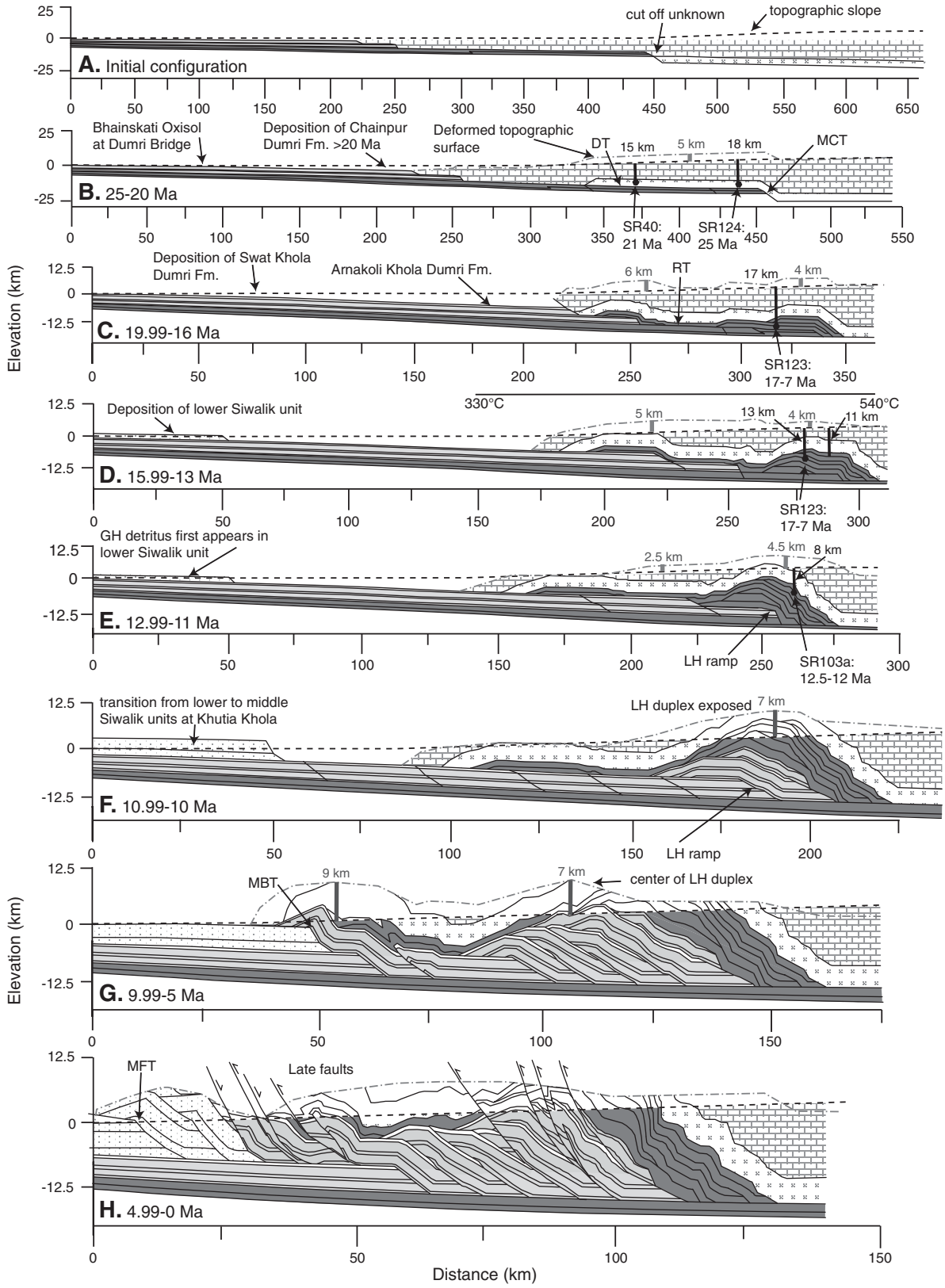

Figure 4. (A–H) Reconstructions from 25 Ma to 0 Ma along the straight line in Figure 1B. Black dashed line is the topography. Gray dot-dash line is the deformed topography. Black circles are the estimated locations of data at depth. Solid black vertical lines estimate the depth of the sample below sea level. Solid vertical dark-gray lines estimate the vertical thickness of units eroded from the thrust belt, which is listed above the line in italics. In each time frame, the faults that will be moved in the next time frame are shown in the undeformed stratigraphy. Abbreviations are the same as in Figure 2. Shading is the same as Figure 3. GH—Greater Himalaya; LH—Lesser Himalaya.

details, see Kohn et al., 2010). A ca. 500 Ma event has been proposed within Greater Himalaya rocks that may have also affected Lesser Himalaya rocks along the northern Indian margin (DeCelles et al., 2000; Gehrels et al., 2003, 2006; Cawood et al., 2007). However, with these caveats, extensive field mapping of Lesser Himalaya rocks throughout far western Nepal indicates that foliation is parallel to original sedimentary bedding, with sedimentary structures emphasizing that bedding has not been overturned (Robinson and Pearson, 2006). In addition, where preserved, the younger Foreland Basin sequence is parallel to underlying Proterozoic formations (Robinson et al., 2006), highlighting that at least in this part of the Himalaya, the Lesser Himalaya section was not significantly deformed prior to the Himalayan event.

(2) Pre-Himalayan and Himalayan internal deformation of Greater Himalaya rocks. Greater Himalaya rocks are metamorphic rocks with internal folding and faulting, and treating the entire unit as a coherent slab is a gross simplification. To avoid complications with differentiating pre-Himalayan and Himalayan deformation, as well as uncertainties in the magnitude of internal strain within the Greater Himalaya, we treat displacement on the Main Central thrust as just the magnitude needed to account for overlap of Greater Himalaya rocks on Lesser Himalaya rocks. The reconstruction assumes that Greater Himalaya rock north of the Main Central thrust is the same rock contained in the Dadeldhura klippe; thus, the Dadeldhura thrust is also the Main Central thrust (Fig. 3) (Johnson et al., 2001; Johnson, 2005; Pearson and DeCelles, 2005). This assumption places a minimum value on shortening and is the simplest solution. We restore Greater Himalaya rocks at the northern limit of restored Lesser Himalaya rocks (e.g., Robinson et al., 2006), as the original relationship between Lesser Himalaya and Greater Himalaya rocks is uncertain and not preserved. Greater Himalaya rocks have been interpreted as a terrane that accreted onto India during the ~500 m.y. orogenic event (e.g., DeCelles et al., 2000) or as part of a passive margin sequence that was only deformed during the Cenozoic collision (e.g., Myrow et al., 2003, 2010). For the purpose of this reconstruction, the origin of Greater Himalaya rocks is not a critical factor, but rather the location in the crust from which they were translated. The maximum southward extent of the Greater Himalaya rocks must be north of restored Lesser Himalaya rocks on the Greater Indian margin.

(3) Pre-Himalayan geometry of Tethyan Himalaya rocks. The sparsely exposed Gondwana sequence through western Nepal is assumed to thicken to the north and become part of the Cambrian–Ordovician through Cretaceous Tethyan Himalaya rocks, which overlay Greater Himalaya rocks precollision. In far western Nepal, the age of the Tethyan Himalaya rocks north of the South Tibetan Detachment system (STDS) is not clear. To the east of this reconstruction in the Simikot region, Murphy and Copeland (2005) identified basal Tethyan Himalaya rocks as Cambrian–Ordovician in age. Another unknown factor is the full thickness of the Tethyan Himalaya stratigraphic section. Available data suggest a thickness of 17–20 km (Ratschbacher et al., 1994; Zhang and Guo, 2007) north of the STDS. Thus, in our reconstruction, Tethyan Himalaya rocks are assumed to reach thicknesses of 17 km at their northern extent, and directly overlie Greater Himalaya rocks. For our original configuration, we show a gently north-dipping (1.5°) Indian passive margin, where Cretaceous rocks are at approximate sea level from the modern foreland to the northernmost extent of the restoration.

Early Himalayan Deformation

Most researchers agree that the Himalayan collision began at ca. 55 Ma (see review in Najman, 2006), with many studies preferring an age of 52–50 Ma (e.g., Zhu et al., 2005; Green et al., 2008; Dupont-Nivet et al., 2010; Najman et al., 2010; Wang et al., 2011). Prior to 25 Ma, an entire thrust belt was built from Tethyan Himalaya strata, the Tibetan thrust belt, as the Indian margin shortened and thickened from ca. 55–25 Ma (Ratschbacher et al., 1994; Murphy and Yin, 2003; Leech et al., 2005; Ding et al., 2005; Webb et al., 2011). Presumably, southward propagation of these deformed Tethyan Himalaya rocks facilitated the burial of Greater Himalaya rocks to their peak temperature and pressure conditions (Patel et al., 1993; Robinson et al., 2003; Murphy and Yin, 2003; Ding et al., 2005; Aikman et al., 2008; Webb et al., 2011). However, because of the remote nature of the Tethyan Himalaya rocks in far western Nepal and Tibet, studies of the Tibetan fold-and-thrust belt are lacking. Thus, the burial depth of Greater Himalaya rocks and the magnitude of shortening accommodated within the Tethyan Himalaya system are unknown.

Topography

Estimating topography through time is fraught with uncertainties; thus, we use a very simple approach to estimating the evolution of topography. To be able to estimate both the topographic load as well as the amount of material removed though erosion, we assume a constant topographic slope from 0 to 4.5 km over a 150 km width, modeled after the modern topographic slope of the Himalaya (e.g., Bookhagen and Burbank, 2006). The transition from no topography to a simple topographic gradient begins at the frontal thrust for a specific time period. The assumption that the Tibetan Plateau had reached its modern height in the part of Tibet north of far western Nepal by 25 Ma is supported by the Nima basin in central Tibet, which indicates an arid climate and high paleoelevations of 4.5–5 km by 26 Ma (DeCelles et al., 2007), as well as negligible exhumation of the region from ca. 45 Ma to present (Hetzel et al., 2011; Rohrmann et al., 2012). An early Himalayan fold-and-thrust belt with a northward-increasing critically tapered slope overlying the Greater Himalaya rocks at the start of the deformation is supported by prograde monazite ages within Greater Himalaya rocks, which indicate burial from 30 to 20 Ma in the Langtang region of central Nepal (Kohn et al., 2004). To test the effect of our topographic assumptions on both the flexural evolution of the Himalayan foreland basin and estimates of erosion, we produced a series of models that are discussed with our simplified topography model in the methods section.

Model Parameters

We bracketed the time steps based on the available synorogenic and hinterland data. Although the data are sparse, seven specific well-dated windows of time bracket magnitudes of deformation documented in sequential reconstructions (Table 3).

A paleosol developed on the exposed Bhainskati Formation at the southern limit of the foreland basin (an exposed forebulge; Fig. 4B) from 40 Ma to ca. 20 Ma (DeCelles et al., 1998b) sets the initial width of the foreland basin after motion on the Main Central thrust ca. 25–21 Ma. These data are from Dumri Bridge in south-central Nepal; although the paleosol is not present in Swat Khola, we use the description at Dumri Bridge because these observations are along strike with the Swat Khola Dumri Formation section. The restored distance between the front of the Main Central thrust after 125 km of motion and the documented paleosol in the Bhainskati Formation is ~260 km. One major factor that controls the width of the foreland basin is the flexural rigidity of the Indian plate (e.g., Jordan and Watts, 2005). Thus, we would predict a match between the estimated width of the foreland basin based on geological constraints, from both foreland basin sediments (thickness, sedimentology, and age) and structure (restored distance between the thrust front and foreland basin deposits), and the estimated width of the basin from flexural modeling of the thrust load. Flexural rigidity and effective elastic thickness (*Te*)

TABLE 3. CHOOSING TIME STEPS

Time step	Significance	Bracketed by
25–20 Ma	Initiation of exhumation within GH rocks interpreted as initiation of MCT	Ar data
19.99–16 Ma	Known deposition of Dumri Formation at 20 Ma (may be older); LH rocks cool through $^{40}Ar/^{39}Ar$ (muscovite)	Magnetostratigraphy; Ar data
15.99–13 Ma	Youngest known Dumri Formation at 15 Ma; begin deposition of Siwalik Group	Magnetostratigraphy
12.99–11 Ma	Lower LH rocks cool through $^{40}Ar/^{39}Ar$ (muscovite)	Ar data
10.99–10 Ma	Exposure of LH rocks at the surface	Isotopic data
9.99–5 Ma	LHD continues to build; MBT by 5–4 Ma	Kinematic reconstruction
4.99–0 Ma	SHTS forms; late faults added to reconstruction	Map patterns

Note: Abbreviations as in Figures 1 and 2.

are two parameters that provide a measure of the long-term strength of the lithosphere (Jordan and Watts, 2005). *Te* is related to the flexural rigidity through estimates for Young's modulus and Poisson's ratio (Turcotte and Schubert, 1982).

The reconstruction program, 2D Move, allows the user to estimate the flexural isostatic deflection of the lithosphere based on the load generated in a sequential reconstruction. The parameters used in the flexural modeling include: effective elastic thickness (*Te*), mantle density, load density, and Young's modulus. Although any of these parameters may be changed in successive time steps, our goal was to choose parameters supported by published gravity models (Lyon-Caen and Molnar, 1985; Jordan and Watts, 2005) and find a self-consistent model that accurately reproduces the basin history. Throughout the model we present here, to model the Eocene–early Miocene flexural rigidity, we used a *Te* of 70 km (Jordan and Watts, 2005), which is approximately equal to a flexural rigidity (D) of 2×10^{24} and is between the values 7×10^{23} and 3×10^{24} used by DeCelles et al. (1998b). Mantle density was set at 3300 kg/m^3, while the load density was estimated at 2700 kg/m^3. Young's modulus was set at 0.7×10^5 MPa.

METHODS

To create the time steps shown in Figure 4, the displacement along the faults was moved sequentially, with both the overlying strata and topography deformed from motion on underlying faults. The deformed topographic surface (area above sea level, gray dot-dash lines on Fig. 4) was modeled as the top of the load, and the base of the load was sea level. For each step, we calculated the isostatic difference from our initial condition with the top of the Cretaceous at sea level. After the program calculated flexural compensation of the load, a new topographic profile was drawn starting at sea level from the southernmost extent of the load and reaching 4.5 km, 150 km to the north (black dashed lines on Fig. 4). Any material above this topographic surface was assumed to have been removed by erosion (area not filled in with a pattern on Fig. 4). Rock that passed through this erosion surface is not included as part of the load put on the plate in the subsequent steps. In each time step, this scenario was repeated, with the new topographic surface being deformed by the southward-propagating deformation, the deformed topographic surface acting as the load, isostatic compensation, and a new topographic surface being generated, above which material was removed by erosion. The eroded material is the area between the deformed topographic surface (the load) and the new topographic slope. The flexure of the plate produced an accommodation space found at the front of the thrust belt into which the synorogenic sediments were shed. Any region below sea level was assumed to be collecting synorogenic sediment. We then compared the thickness of synorogenic sediment at locations where geologic constraints from the foreland basin exist. The critical components that we needed the model to match were the location and depth of foreland basin data, the dip of the décollement, and the exposure of rocks mapped at the surface today. Detailed data from the Dumri Formation (ca. 20–15 Ma) and the Siwalik Group sediments (15 Ma to present), presented previously and summarized in Table 1, were used as constraints for checking both the southern extent of the load and the flexural isostatic parameters as the model developed through time. The final model needed to have a décollement dip consistent with that identified for the Main Himalayan thrust (Ni and Barazangi, 1984; Pandey et al., 1999).

To test the effect of our simplified topographic assumption, we repeated the method steps varying topography, *Te*, and the density of the load to find the solutions that matched the location and depth of foreland basin data, the dip of the décollement, and the exposure of rocks mapped at the surface today. Because increasing topography and/or density increases the load while an increase in *Te* supports that load, there are several variations of topography (1°–3° uniform slopes as well as nonuniform slopes), density (2600–2800 kg/m^3), and values of *Te* (45–90) that matched the available constraints. Thus, the absolute value of these variables is not critical or unique for the model. However, within these variations, every scenario that matched our constraints of location and depth of foreland basin data, the dip of the décollement, and the exposure of rocks mapped at the surface today produced a similar history for both the magnitude of exhumation and depth and migration of the foreland basin. Using a best-fit "no topography" model decreased foreland basin thickness (by 1.5–2 km), shallowed the position of the décollement by 1°–1.5°, and increased the magnitude of material removed (2 km). Thus, the rock that was at the surface did not match the data from the hinterland and foreland and highlighted that there are limits to permissible variations in topography, *Te*, and the density. These sensitivity tests illustrated that while our models are nonunique, the first-order patterns of the location and timing of exhumation and deposition of sediments are controlled by the evolving structural load (Fig. 4). The similarity in the exhumation estimates argues that the largest control on location, time, and amount of exhumation is the vertical component of deformation (Whipp et al., 2007).

We used thermochronologic data from the hinterland to compare the magnitude of exhumation proposed in our model to that measured with available thermochronometers. The closure temperature for any mineral system depends on the exhumation rate (e.g., Brandon et al., 1998), while the depth of that closure temperature is a function of both exhumation rate and the original geothermal gradient. The thermochronologic data for far western Nepal are too meager to warrant detailed thermodynamic modeling; thus, to compare the data to our model, we obtained an average closure temperature from the literature and then used the predicted depth of the sample to calculate the necessary geothermal gradient required to match the data to the model. This approach is not intended to solve for the gradient or make a robust calculation of exhumation, but simply to provide enough information to evaluate whether the match is viable.

RECONSTRUCTIONS

The initial configuration of the sequential model is illustrated in Figure 4A. Due to uncertainties in the geometry, thickness, and extent of Tethyan Himalaya shortening, we only show the undeformed Tethyan Himalaya section. As a result of an undeformed Tethyan Himalaya section, as well as uncertainty in the initial pressure and temperature conditions in far western Nepal, the base of Greater Himalaya rocks is initially at 25 km (17 km Tethyan Himalaya + 8 km Greater Himalaya). Initial topography is displayed with elevation gradually increasing toward the north to 4.5 km. The following time steps were chosen based on the criteria outlined in Table 3.

From 25 to 20 Ma (Fig. 4B) in the foreland basin, the Bhainskati Formation paleosol continued to form at the front of the thrust belt. In Figure 4B, the arrow representing the paleosol points to the top of the Lesser Himalaya sequence because the Bhainskati Formation is only 100 m thick and too thin to be represented on the reconstruction. The Main Central thrust carried Greater Himalaya rock 125 km over the Lesser Himalaya in the Ramgarh thrust sheet. During this time, the northern Lesser Himalaya duplex and Ramgarh thrust sheet were buried, and Lesser Himalaya rocks were metamorphosed (dark-gray color in Fig. 4B). Post erosion, sample SR124, immediately adjacent to the Main Central thrust (25 Ma cooling age), and sample SR40, within the Dadeldhura klippe (21 Ma cooling age), are 18 km and 15 km below the surface, respectively. This suggests a geothermal gradient of 22–30 °C/km to reconcile cooling ages with the erosional history implied by the reconstruction, assuming a 400–450 °C closure temperature for muscovite (Hames and Bowring, 1994). The foreland basin extends southward 90 km (Fig. 4B), ~25 km north of the Bhainskati Formation paleosol described by DeCelles et al. (1998b) at Dumri Bridge. A sample from the Dumri Formation near the village of Chainpur, described earlier, has a detrital mica age of ca. 20 Ma; however, the exact location within the section is unknown. Thus, north of this sample, the Dumri Formation is likely older, 25–20 Ma. The oldest available age on the Dumri Formation is <30 Ma from samples in NW India (Najman et al., 2005).

From 19.99 to 16 Ma (Fig. 4C) in the foreland basin, deposition of the subaerial, fluvial Dumri Formation began at 19.9 Ma at Swat Khola (Ojha et al., 2000, 2009). The Ramgarh thrust was active in several thrust sheets, totaling ~109 km (Robinson et al., 2006). Post motion on the Ramgarh thrust and after erosion, sample SR123 (17–7 Ma cooling age) restores to a depth of 17 km, but remains between 17 and 13 km depth until ca. 12 Ma. The length of time at this depth (~7 m.y.) may explain the complicated age spectra. Using a closure temperature range of 400–450 °C, a closure depth of 17–13 km would suggest geothermal gradients of 25–35 °C/km. Alternatively, the muscovite could represent the age that muscovite grew during dynamic recrystallization while the Ramgarh thrust was active, possibly at temperatures as low as <300 °C (Passchier and Trouw, 1996), as suggested by Robinson et al. (2006). However, maximum temperatures for these rocks measured from Raman spectroscopy of carbonaceous material range from 400 °C to 500 °C (Bollinger et al., 2004; Beyssac et al., 2004). Further support for 400–500 °C maximum temperatures comes from the cooling history of sample SR103a, immediately north of sample SR123. Sample SR103a is from the first Lesser Himalaya thrust sheet under the Main Central thrust, a Ramgarh thrust imbricate, and it cooled rapidly from 12.5 to 12 Ma (Fig. 4E), precluding significantly lower temperatures for sample SR123. The foreland basin created by displacement on the Ramgarh thrust extends to 26 km, and suggests ~0.5 km of Dumri deposition by 16 Ma at Swat Khola. At the same time as thrust faulting was occurring in the thrust belt, normal faulting on the STD occurred in the Tethyan Himalaya. Detrital and geochronological data suggest slip on the STD faults from 20 Ma to 9 Ma (Murphy and Copeland, 2005) in the Simikot region, NW of the village of Chainpur. Because of the uncertainty surrounding the timing and geometry of the STD through time, the fault system is not added to Figure 4. In Figures 4F–4H, the STD at the surface would be at the contact between Greater Himalaya and Tethyan Himalaya rocks.

From 15.99 to 13 Ma (Fig. 4D) in Swat Khola, deposition of the Dumri Formation ended at ca. 15 Ma, and deposition of the lower Siwalik unit occurred from ca. 15 Ma to 10.8 Ma (Ojha et al., 2000, 2009). North of the Dadeldhura klippe, where the Dumri Formation is sandstone, the Ramgarh thrust sheet cuts the Dumri Formation at Arnakoli Khola. Based on the minimum 15 Ma age of the Dumri Formation at Swat Khola, DeCelles et al. (2001) argued that the age of slip on the Ramgarh thrust must be younger than 15 Ma, because that fault cuts the Dumri Formation. Arnakoli Khola is ~130 km north of Swat Khola (see annotation on Fig. 4D). Our model suggests that initial deposition of the Dumri Formation at Arnakoli Khola was as early as 25 Ma, but it becomes cut by the Ramgarh thrust between 16 and 13 Ma. In Khutia Khola, deposition of the lower Siwalik unit began by 13.3 Ma (Ojha et al., 2000); however, in the Karnali River, Gautam and Fujiwara (2000) documented deposition initiating at 16 Ma. Our reconstruction shows deposition of the lower Siwalik unit from 15.99 to 13 Ma in the location of the frontal two thrusts of the Subhimalayan thrust system. Over this time window, the northern Lesser Himalaya duplex continued to build via the emplacement of lower Lesser Himalaya thrust sheets.

From 12.99 to 11 Ma (Fig. 4E), the Lesser Himalaya duplex continued to build by incorporating more of the Paleoproterozoic Lesser Himalaya sequence. The increase in the thickness of material incorporated into the Lesser Himalaya duplex creates a more pronounced structural high and facilitates erosion to expose the highest-grade Greater Himalaya rocks in the hanging wall of the Main Central thrust at the surface. Proterozoic Lesser Himalaya rocks rapidly exhume from ~12 km depth to ~5 km. At the transition between the time steps shown in Figures 4D and 4E, Lesser Himalaya sample SR103a records rapid cooling at ca. 12 Ma. At Khutia Khola, kyanite and sillimanite metasedimentary lithic fragments first appear in the upper portion of the lower Siwalik unit at ca. 11 Ma (DeCelles et al., 1998a). This influx of high-grade metamorphic minerals corresponds with the emplacement of thicker Lesser Himalaya thrust sheets in the Lesser Himalaya duplex.

From 10.99 to 10 Ma (Fig. 4F), the transition from the lower to middle Siwalik unit occurred in Khutia Khola at 10.8 Ma (Ojha et al., 2000). In the hinterland, the first thrust sheet containing the entire Mesoproterozoic Lesser Himalaya sequence is emplaced in the Lesser Himalaya duplex, creating a 7 km ramp in the Main Himalayan thrust. As illustrated in Figure 4F, this structural high has a pronounced effect on the magnitude of erosion immediately above it. This focused erosion exposes Lesser Himalaya rock, creating a new sediment source for the foreland basin. At this time, input from Lesser Himalaya rocks is documented by the change to a more negative ε_{Nd} value (Huyghe et al., 2001; Robinson et al., 2001; Szulc et al., 2006) and the first appearance of Lesser Himalaya–derived carbonate clasts (DeCelles et al., 1998a).

From 9.99 to 5 Ma (Fig. 4G), the middle Siwalik unit continued to be deposited at both Khutia Khola and Karnali River. In the thrust belt, the last three Lesser Himalaya thrust sheets of the Lesser Himalaya duplex were consecutively emplaced, and the locus of thrusting was transferred south of the Dadeldhura klippe, forming the Main Boundary thrust. Emplacement of the Main Boundary thrust, the last Lesser Himalaya thrust sheet, over Subhimalaya rock caused the southern limb of the Dadeldhura klippe to uplift and rotate to the north, giving the Dadeldhura klippe its synclinal shape. DeCelles et al. (1998a) argued for emplacement of the Main Boundary thrust by 4–5 Ma. Map patterns indicate that the Main Boundary thrust

cuts middle Siwalik unit rock (Robinson et al., 2006); thus, some component of motion on the Main Boundary thrust occurred after middle Siwalik unit deposition (ca. 5 Ma). Although no cooling ages exist for the Lesser Himalaya duplex in far western Nepal, in central Nepal and NW India, pre-Cenozoic $^{40}Ar/^{39}Ar$ cooling ages are prevalent in the Lesser Himalaya duplex and in rocks carried by later thrusts to the south (Catlos et al., 2001; Wobus et al., 2003; Bollinger et al., 2004; Kohn et al., 2004; Célérier et al., 2009), suggesting that samples were not buried deeply enough during the Cenozoic orogeny to completely reset muscovite ages.

From 4.99 to 0 Ma (Fig. 4H) in Khutia Khola, the upper Siwalik unit was deposited at a projected time of 4.5 Ma (Ojha et al., 2000). The upper Siwalik unit is a proximal facies that contains large Lesser Himalaya conglomerate clasts, suggestive of an immediate source to the north (DeCelles et al., 1998b). South of the Main Boundary thrust, the Subhimalayan thrust system forms exclusively within Subhimalaya rocks. Slip on the Main Frontal thrust may have begun at ca. 2 Ma and continues in Karnali River (van der Beek et al., 2006). After the end of the major deformation sequence in the thrust belt, eight small-scale thrust and normal faults with less than 5 km of displacement were added to the reconstruction program based on field relationships (see Robinson, 2008). Because the sequence and timing are difficult to determine and the offsets are less than 5 km, only the end result is shown.

MAGNITUDES AND VARIATIONS OF EROSION

The gray dot-dash lines on Figure 4 represent the deformed topographic surface. The rock removed by erosion in each time step is estimated as the difference between the deformed topographic surface and the new topographic profile drawn after flexural compensation of the load (black dashed lines on Fig. 4) (see area, Table 4). To produce a denudation rate estimate, both the duration of exhumation and the length scale over which that denudation was applied are needed (Barnes and Pelletier, 2006; McQuarrie et al., 2008). Duration is the length of each frame in Figure 4. The length-scale is the distance along the cross section where rock was "removed" via erosion in the model. The thickness of material removed (exhumation amount) is calculated by dividing the area by the length. The exhumation rate is calculated by dividing the exhumation amount by the duration. Exhumation is a result of either erosion (rivers, glaciers, or landslides) or normal faulting. Only minor normal faulting has affected the thrust belt in far western Nepal (Robinson et al., 2006; Robinson, 2008). Figure 4H illustrates two normal faults that were added in at the end of the reconstruction and that match faults observed in the field. These faults have less than 5 km of offset and are located between the Main Boundary thrust and southern Dadeldhura thrust in the Lesser Himalaya imbricate zone. The ages of these faults are unknown. Because the offsets are small and do not appear in consecutive cross sections along strike (Robinson et al., 2006), we attribute the rate of removal to erosion.

TABLE 4. MAGNITUDE OF EROSION

Figure	Age range (Ma)	Area (km^2)	Duration (m.y.)	Length (km)	Exhumation amount (vertical km)	Rate of exhumation (mm/yr)
Fig. 4B	25–20	641	5	130	4.93	0.99
Fig. 4C	19.99–16	384	4	130	2.95	0.74
Fig. 4D	15.99–13	372	3	123	3.02	1.0
Fig. 4E	12.99–11	241	2	85	2.84	1.4
Fig. 4F	10.99–10	323	1	77	4.20	4.2 (2.1*)
Fig. 4G	9.99–5	541	5	120	4.51	0.90 (1.1*)
Fig. 4H	4.99–0	515	5	133	3.87	0.77
		2285†	25	119	19.2	0.77

*Using 10.99–9 Ma and 8.99–5 Ma; see text for discussion.
†Average area calculated along the reconstruction line with a duration of 25 m.y. and the length being the final length of the Chainpur cross section (Robinson et al., 2006), exhumation amount is area divided by length, and the rate of exhumation is exhumation amount divided by duration.

The rate of erosion we calculate varies from 0.7 to 4.2 mm/yr, with most estimates between 0.7 and 1.4 mm/yr (Table 4), comparable to exhumation estimates across the Himalaya and particularly close in magnitude to estimates obtained in western Nepal (Table 5). Figure 4F, from 10.99 to 10 Ma, has an anomalously high rate of erosion (4.2 mm/yr) when compared to periods of time before and after, and it also has the shortest duration. This erosion rate increase occurs when ~20 km of overburdened is thrust over a 7 km ramp in the Main Himalayan thrust and exposes Lesser Himalaya rock at the surface. The time window over which that happens is not exact; however, sedimentological constraints from Khutia Khola require a Lesser Himalaya source at 10.8 Ma. Thus, at least half of the erosion must be before 10 Ma. By extending the time window 1 m.y., from 10.99 to 9 Ma (see asterisk in Table 4), the exhumation rate drops to 2.1 mm/yr, and the erosion rate in the subsequent time step increases to 1.1 mm/yr. In general, the rate of erosion is fairly constant through the emplacement of major thrust sheets, and more minor faults in far western Nepal. The notable increase in erosion is linked to the creation and southward propagation of 7-km-thick ramps that built the southern half of the Lesser Himalaya duplex.

TABLE 5. COMPARISON OF EXHUMATION RATES

Location	Technique	Rate (mm/yr)	Duration (m.y.)	Reference
Karnali River, western Nepal	Detrital zircon fission-track ages	1.4 ± 0.2	11–0	Bernet et al. (2006)
Western and central Nepal	Detrital white mica $^{40}Ar/^{39}Ar$ ages	1.4–2.0	10–0	Szulc et al. (2006)
		2.0–2.5	13–10	
		3.6	16	
Marsyandi River, central Nepal	Apatite fission-track ages	>2–5	2–0	Burbank et al. (2003)
Western Himalaya	Geochemical analyses	2.9	Modern	Galy and France-Lanord (2001)
Eastern Himalaya	Geochemical analyses	2.1	Modern	
Marsyandi River, central Nepal	Bedrock apatite fission-track ages	1.5	2–0.8	Blythe et al. (2007)
		2.5–5	0.8–0	
Gosainkund profile, central Nepal	Apatite fission-track ages	2.0–2.5	2–0?	Robert et al. (2009)
Sutlej River, northern, northwest India	Apatite and zircon fission-track ages; detrital white mica	2–3	23–19; 3–0	Thiede et al. (2009)
		0.4–0.8	19–3	
Sutlej River, southern, northwest India	Apatite and zircon fission-track ages; detrital white mica	2–3	11–2	Thiede et al. (2009)

We can compare our estimates of magnitude and rates of erosion to published estimates through the region (Tables 4 and 5). Bernet et al. (2006) used detrital zircon fission track on samples from Karnali River to determine rates of exhumation, and they reported evidence for widespread cooling at ca. 16.0 ± 1.4 Ma, with continuous exhumation at a rate of ~1.4 ± 0.2 km/m.y. Bernet et al. (2006) reported a 4 m.y. lag time between the youngest statistic peaks in the samples from the age of the sediment. The youngest statistic peak from 14 Ma sediments is 18.7 ± 3.2 Ma, and from 12 Ma sediments, it is 16.5 ± 2.2 Ma. The zircon fission-track system closure temperature is ~240 °C, yielding orogenic cooling rates of 15 °C/m.y. (Hurford, 1986; Brandon et al., 1998). Using our model, we can estimate the magnitude of vertical exhumation between these two time windows. From 19 to 14 Ma, an 8–11 km thickness of rock was removed, while from 16 to 12 Ma, 7.5–8.5 km of rock were removed. Assuming a 240 °C closure temperature, our model would suggest geothermal gradients of 22–32°/km to account for the exhumation and then deposition of these minerals. In addition, we can compare times of pronounced exhumation. As discussed previously, from 10 to 11 Ma exhumation dramatically increased due to the development of a significant ramp and the associated vertical component of deformation. Using the lag time of detrital muscovite, Szulc et al. (2006) showed the highest exhumation rates are between 13 and 10 Ma, with rates between 2 and 2.5 mm/yr. Our rates are also the highest over this window of time, with rates that range from 1.4 to 2.1 mm/yr and possibly as high as 4.2 mm/yr.

Table 5 compares the available exhumation rates from across the Himalaya. What becomes quickly visible is that exhumation rates from 2 Ma to the present are notably higher in central Nepal and NW India than the youngest rate (5–0 Ma) that we propose here. Measurements of Quaternary features in central Nepal indicate rates of exhumation as high as 2–5 mm/yr, similar to modern rates (2–3 mm/yr) inferred from river geochemistry (Galy and France-Lanord, 2001). Thiede et al. (2009) also suggested faster exhumation rates (2–3 mm/yr) from 3 to 0 Ma. Two possible explanations exist for this discrepancy. One is that our broad-brush approach for determining magnitudes of exhumation is not sensitive to a recent (2–0 Ma) increase in exhumation that would be best illustrated with a lower-temperature thermochronometer system like apatite fission track. Our approach averages out exhumation both temporally (5 Ma to present) as well as spatially (Fig. 4). More discrete regions on Figure 4 may have lost up to 7 km of vertical overburden within the past 5 m.y., indicating potential exhumation rates of 1.4 mm/yr. If most of that erosion happened in the past 2–3 m.y., rates could be as high as 2–3.5 mm/yr. The second possibility is that deformation and associated exhumation vary spatially with time along the Himalayan arc. Thiede et al. (2009) showed how exhumation rates vary with time in the Sutlej River valley in NW India, with times of fast exhumation (2–3 mm/yr) that fall between 23 and 19 Ma and 11–0 Ma. The window of time in our study that highlights the fastest exhumation (ca. 13–10 Ma) is a period of slower exhumation in Thiede et al. (2009). Their highest exhumation rates start at 11 Ma but are more focused around 6–4 Ma. Presently, we just do not have the data necessary to differentiate between these two hypotheses.

RATES AND VARIATIONS OF SHORTENING

Table 6 shows the amount of shortening in each time period as highlighted in Figure 4. The shortening amount is derived from both balanced cross sections (Robinson et al., 2006) and 2D Move reconstructions detailed in Robinson (2008). The rate is calculated by dividing the shortening amount by the duration. The timing of the late faults (shown in Fig. 4H) is unknown, although they must postdate the faults they cut. The 10.6 km total offset for these faults listed here is the magnitude achieved by adding and subtracting the offset on the thrust and normal faults, respectively. Adding the total magnitude of the late fault displacement to the smallest rates (Figs. 4D and 4H) only increases the rate by 2–4 mm/yr. Thus, with that logic, the error on the rates is ~3 mm/yr.

TABLE 6. SHORTENING RATES

Figure	Age range (Ma)	Fault name	Duration (m.y.)	Shortening (km)	Rate (mm/yr)
Fig. 4B	25–20	MCT	5	125	25
Fig. 4C	19.99–16	RT	4	108.8	27
Fig. 4D	15.99–13	LHD	3	42.7	14
Fig. 4E	12.99–11	LHD	2	66.1	33
Fig. 4F	10.99–10	LHD	1	26.7	27
Fig. 4G	9.99–5	LHD, MBT	5	63.4	13
Fig. 4H	4.99–0	SHTS	5	21.4	4
Subtotal				485.9	
Late faults				10.6	
Total			25	496.5	20

Note: Abbreviations as in Figures 1 and 2.

Between 25 and 16 Ma and 13 and 10 Ma, the shortening rate averages ~27 mm/yr, with shortening rates as high as 33 mm/yr from 13 to 11 Ma (Table 6). In contrast, from 16 to 13 Ma and 10 to 5 Ma, shortening rates are 13–14 mm/yr. From 5 to 0 Ma, shortening rates are 4 mm/yr. Even summing all of the shortening accommodated by the last-stage faults, shortening rates during the last time period (5–0 Ma) are still low (6.4 mm/yr). The slowing of shortening post–5 Ma is a function of the age of displacement on the Main Boundary thrust. The Main Boundary thrust cuts the middle Siwalik unit, indicating that some component of displacement occurred post–5 Ma. An alternative interpretation of the Main Boundary thrust and recent rates is to combine displacement from 10 Ma to present, for an 8.5 mm/yr shortening rate, possibly as high as 9.6 mm/yr, if all of the late-stage faults developed during this time.

The average rate of shortening from 25 Ma to the present is calculated by dividing the total shortening by the total duration, providing a long-term average of 20 mm/yr. This rate agrees with active global positioning system (GPS) shortening rates across the Himalaya of 15–20 mm/yr (e.g., Bettinelli et al., 2006), as well as the Holocene rates of 21.5 ± 2 mm/yr slip rate on the Main Frontal thrust determined from deformed Holocene terraces (Lavé and Avouac, 2000). The matches among the long-term rate, Holocene rates, and GPS rates led to the prevailing assumption that the shortening rate along the Main Himalayan thrust has been constant through time (e.g., Herman et al., 2010). However, Table 6 shows that the rate of shortening varies significantly through time, leading to periods of India-Asia convergence where more or less deformation is being accommodated by the Indian plate, as well as pulsed propagation of the thrust front. The amount of convergence accommodated by India is greater during emplacement of the Main Central thrust, Ramgarh thrust, and during the middle stage of Lesser Himalaya duplex development. The rate is slower during the initial building of the northern Lesser Himalaya duplex, when the first few thrust sheets are being emplaced over smaller ramps in the Main Himalayan thrust and as the toe of the thrust belt propagates to the south, forming the Main Boundary thrust and Subhimalayan thrust system.

IMPLICATIONS

Previous to this study, balanced cross sections through the Himalaya were used to provide a long-term average of shortening solely from the initiation of motion on the Main Central thrust to present. By linking both

hinterland and foreland data to the emplacement of major structures, we present a method with which to extract a more detailed view of shortening rates and how they vary through time. What emerges is a tempo of deformation that varies, with periods of rapid shortening during the propagation of the Main Central thrust and development of the Lesser Himalaya duplex (~30 mm/yr). Both early (after the emplacement of the Ramgarh thrust) and late stages of Lesser Himalaya duplex development are marked by windows of slow shortening (~13–14 mm/yr). As noted by Rahl et al. (2011) in the Pyrenees, fault activity occurs in pulses, with slip occurring contemporaneously on multiple faults throughout the wedge. This reconstruction of fault activity and erosion suggests that orogenic wedges may not evolve in a steady fashion but instead exhibit significant changes in rates of deformation.

An important implication of varying shortening rates is that the partitioning of deformation within the India-Asia collision zone may have changed through time. If the result of 30+ mm/yr of motion of individual faults is robust, then that means that certain faults (Main Central thrust, Ramgarh thrust, and middle stage of Lesser Himalaya duplex development) accommodated a significant component of the 55–40 mm/yr India-Asia convergence rates (e.g., Copley et al., 2010). The approach we use here can be also applied to other orogens with robust data sets in the foreland and hinterland (e.g., Appalachians, Andes, and western United States) to evaluate the presence and possible mechanisms for variations in shortening rates. While proposing variable shortening through time is a new view of Himalayan deformation, it has been documented in other orogens. Linking detailed cross sections with a well-dated foreland basin showed shortening variations between 4 and 13 mm/yr over the past 8 m.y. in the Subandean fold-and-thrust belt of Argentina (Echavarria et al., 2003). Over longer times scales (45 Ma to present), shortening rates though the central Andes have also varied between 4 and 13 mm/yr (McQuarrie et al., 2005; Oncken et al., 2006), although integrating detailed basin studies, thermochronology, and structure with a linked structural and flexural model may facilitate extracting a more detailed history of shortening and exhumation for this region as well.

Using balanced cross sections to determine exhumation has also been limited to long time scales averaged over the duration of deformation due to the uncertainty in partitioning the details of exhumation magnitude with time (Barnes and Pelletier, 2006; McQuarrie et al., 2008). However, by accounting for flexure and making reasonable assumptions about the topographic slope in the past, we can calculate first-order denudation magnitudes through time that can be compared to both thermochronometer systems as well as the associated basin history. This approach is particularly powerful in the Himalaya because the Himalayan foreland basin has preserved minerals and isotopic signatures that can be linked to specific tectonostratigraphic packages.

Exhumation is most strongly linked to the vertical component of deformation (e.g., Whipp et al., 2007), and sequentially restored balanced cross sections are the most accurate models for the locations of active ramps in the past. By linking the sequentially restored cross sections to spatially constrained areas of rapid uplift, we can test the accuracy of the geometry displayed in the balanced cross sections. To a first order, the presence and location of the Lesser Himalaya ramps are supported by the exhumation history. An obvious benefit to linking sequentially restored cross sections to thermochronometry and basin development is that these two data sets provide temporal constraints on the deformation. The only way to determine rates is to link the shortening calculated in the fold-and-thrust belt to the time over which that shortening happens. In this study, exhumation appears consistent except for a period from 10 to 13 Ma, which exhibits an increase in exhumation. This coincides with the development of a 7 km ramp in the Main Himalayan thrust that lifted the overburden to the erosional surface. Thus, development of structures with a significant vertical component affects the exhumation rate.

CONCLUSIONS

This study is the first to fully integrate deformation and erosion of the fold-and-thrust belt with flexure of the foreland basin to produce a three-dimensional model, length, height, and time, of the unroofing of the central Himalaya. The result is the ability to link magnitudes of shortening and exhumation to the concurrent deposition within the linked foreland basin–thrust belt system.

A shift in provenance from only Greater Himalaya–Tethyan Himalaya contribution to sediment that contains Lesser Himalaya input is widely recognized in the central Himalaya at ca. 10 Ma. We illustrate that during this time period, Lesser Himalaya and Greater Himalaya rocks were lifted over a large (7 km) Lesser Himalaya ramp. The ramp in the Main Himalayan thrust caused Lesser Himalaya rocks to be elevated, focused erosion in this region, and allowed eroded Lesser Himalaya sediment to be deposited in the Siwalik Group.

In previous studies, it was suggested that Greater Himalaya rocks were exposed by 20 Ma, providing sediment into the foreland basin. By analyzing the data without a bias and by using the hinterland and foreland basin data in combination with the reconstruction, we found that Greater Himalaya rocks were not exposed until ca. 12 Ma along the reconstruction line.

The average shortening rate is ~20 mm/yr, similar to other studies. However, by identifying critical windows of time that can be accurately dated, we bracket the magnitude of shortening that occurs in these windows of time. What is illuminated is a shortening rate that has varied significantly through time. The highest rates from 25 to 33 mm/yr were during emplacement of the Main Central thrust, Ramgarh thrust, and the middle part of the Lesser Himalaya duplex. After emplacement of the Ramgarh thrust, the early and late stages of Lesser Himalaya duplex development are marked by windows of slow shortening (~13–14 mm yr) as well as formation of the Main Boundary thrust and Subhimalayan thrust system.

By accounting for both flexure and an evolving topography with time, we can estimate the magnitude of denudation and obtain exhumation rates. The exhumation history we elucidate through our model is consistent with bedrock and detrital thermochronology obtained through the region. Our average exhumation rates are within the values obtained by other studies in the Himalaya, validating the techniques and assumptions used in the model. Even though our approach allows us to get the most information out of existing data, our understanding of the deformation and exhumational history of far western Nepal is still limited by a lack of data. Future work combining more detailed thermochronology and reconstructions that extend along the Himalayan arc can illuminate the four-dimensional mountain building in the Himalaya, providing a more detailed database for dynamic models.

ACKNOWLEDGMENTS

Informal discussions regarding the data presented were held with P. DeCelles, A. Martin, and O. Pearson. Reviews of an early version of this manuscript were provided by D. Burbank, P. van der Beek, and an anonymous reviewer. Reviews of this manuscript were provided by An Yin, an anonymous reviewer, and Editor John Goodge. Robinson acknowledges support from Cooperative Institute for Research and Science (CIRES) at the University of Colorado at Boulder. McQuarrie received support from the Alexander von Humboldt Foundation. Robinson and McQuarrie thank Midland Valley for the use of the program 2D Move.

REFERENCES CITED

Aikman, A.B., Harrison, T.M., and Ding, L., 2008, Evidence for early (>44 Ma) Himalayan crustal thickening, Tethyan Himalaya, southeastern Tibet: Earth and Planetary Science Letters, v. 274, p. 14–23, doi:10.1016/j.epsl.2008.06.038.

Amatya, K.M., and Jnawal, B.M., 1994, Geological Map of Nepal: Kathmandu, Nepal, Royal Department of Mines and Geology, scale 1:1,000,000, 1 sheet.

Amidon, W.H., Burbank, D.W., and Gehrels, G.E., 2005, Construction of detrital mineral populations: Insights from mixing of U/Pb zircon ages in Himalayan rivers: Basin Research, v. 17, p. 463–485, doi:10.1111/j.1365-2117.2005.00279.x.

Barnes, J.B., and Pelletier, J.D., 2006, Latitudinal variation of denudation in the evolution of the Bolivian Andes: American Journal of Science, v. 306, p. 1–31, doi:10.2475/ajs.306.1.1.

Bernet, M., van der Beek, P., Pik, R., Huyghe, P., Mugnier, J.-L., Labrin, E., and Szulc, A., 2006, Miocene to recent exhumation of the central Himalaya determined from combined detrital zircon fission-track and U/Pb analysis of Siwalik sediments, western Nepal: Basin Research, v. 18, no. 4, p. 393–412, doi:10.1111/j.1365-2117.2006.00303.x.

Bettinelli, P., Avouac, J.-P., Flouzat, M., Jouanne, F., Bollinger, L., Willis, P., and Chitraker, G., 2006, Plate motion of India and interseismic strain in the Nepal Himalaya from GPS and DORIS measurements: Journal of Geodesy, v. 80, p. 567–589, doi:10.1007/s00190-006-0030-3.

Beyssac, O., Bollinger, L., Avouac, J.P., and Goffe, B., 2004, Thermal metamorphism in the Lesser Himalaya of Nepal determined from Raman spectroscopy of carbonaceous material: Earth and Planetary Science Letters, v. 225, p. 233–241, doi:10.1016/j.epsl.2004.05.023.

Blythe, A., Burbank, D.W., Carter, A., Schmidt, K.L., and Putkonen, J., 2007, Plio-Quaternary exhumation history of the central Himalaya: 1. Apatite and zircon fission track and apatite [U-Th]/He analyses: Tectonics, v. 26, TC3002, doi:10.1029/2006TC001990.

Bollinger, L., Avouac, J.P., Beyssac, O., Catlos, E.J., Harrison, T.M., Grove, M., Goffe, B., and Sapkota, S., 2004, Thermal structure and exhumation history of the Lesser Himalaya: Tectonics, v. 23, TC5015, doi:10.1029/2003TC001564.

Bookhagen, B., and Burbank, D.W., 2006, Topography, relief, and TRMM-derived rainfall variations along the Himalaya: Geophysical Research Letters, v. 33, L08405, doi:10.1029/2006GL026037.

Boyer, S.E., and Elliott, D., 1982, Thrust systems: The American Association of Petroleum Geologists Bulletin, v. 66, p. 1196–1230.

Brandon, M.T., Roden-Tice, M.K., and Garver, J.I., 1998, Late Cenozoic exhumation of the Cascadia accretionary wedge in the Olympic Mountains, northwest Washington State: Geological Society of America Bulletin, v. 110, p. 985–1009, doi:10.1130/0016-7606(1998)110<0985:LCEOTC>2.3.CO;2.

Brunel, M., 1986, Ductile thrusting in the Himalayas: Shear sense criteria and stretching lineation: Tectonics, v. 5, p. 247–265, doi:10.1029/TC005i002p00247.

Burbank, D.W., Beck, R.A., and Mulder, T., 1996, The Himalayan foreland basin, *in* Yin, A., and Harrison, T.M., eds., Tectonics of Asia: New York, Cambridge University Press, p. 205–226.

Burbank, D.W., Blythe, A.E., Putkonen, J., Pratt-Sitaula, B., Gabet, E., Oskin, M., Barros, A., and Ojha, T.P., 2003, Decoupling of erosion and precipitation in the Himalayas: Nature, v. 426, p. 652–655, doi:10.1038/nature02187.

Cande, S.C., and Kent, D.V., 1995, Revised calibration of the geomagnetic polarity timescale for the Late Cretaceous and Cenozoic: Journal of Geophysical Research, v. 100, p. 6093–6095, doi:10.1029/94JB03098.

Catlos, E.J., Harrison, T.M., Kohn, M.J., Grove, M., Ryerson, F.J., Manning, C., and Upreti, B.N., 2001, Geochronologic and thermobarometric constraints on the evolution of the Main Central thrust, central Nepal Himalaya: Journal of Geophysical Research, v. 106, p. 16,177–16,204, doi:10.1029/2000JB900375.

Cawood, P.A., Johnson, M.R.W., and Nemchin, A.A., 2007, Paleozoic orogenesis along the Indian margin of Gondwana: Tectonic response to Gondwana assembly: Earth and Planetary Science Letters, v. 255, p. 70–84, doi:10.1016/j.epsl.2006.12.006.

Célérier, J., Harrison, T.M., Yin, A., and Webb, A.A.G., 2009, The Kumaun and Garwhal Lesser Himalaya, India: Part 1: Structure and stratigraphy: Geological Society of America Bulletin, v. 121, p. 1262–1280, doi:10.1130/B26344.1.

Chapple, W.M., 1978, Mechanics of thin-skinned fold-and-thrust belts: Geological Society of America Bulletin, v. 89, p. 1189–1198, doi:10.1130/0016-7606(1978)89<1189:MOTFB>2.0.CO;2.

Copley, A., Avouac, J.-P., and Royer, J.-Y., 2010, India-Asia collision and the Cenozoic slowdown of the Indian plates: Implications for the forces driving plate motions: Journal of Geophysical Research, v. 115, B03410, doi:10.1029/2009JB006634.

Dahlen, F.A., 1990, Critical taper model of fold-and-thrust belts and accretionary wedges: Annual Review of Earth and Planetary Sciences, v. 18, p. 55–99, doi:10.1146/annurev.ea.18.050190.000415.

Daniel, C.G., Hollister, L.S., Parrish, R.R., and Grujic, D., 2003, Exhumation of the Main Central thrust from lower crustal depths, eastern Bhutan Himalaya: Journal of Metamorphic Geology, v. 21, p. 317–334, doi:10.1046/j.1525-1314.2003.00445.x.

Davis, D., Suppe, J., and Dahlen, F.A., 1983, Mechanics of fold-and-thrust belts and accretionary wedges: Journal of Geophysical Research, v. 88, p. 1153–1172, doi:10.1029/JB088iB02p01153.

DeCelles, P.G., and Giles, K.N., 1996, Foreland basin systems: Basin Research, v. 8, p. 105–123, doi:10.1046/j.1365-2117.1996.01491.x.

DeCelles, P.G., Gehrels, G.E., Quade, J., Kapp, P.A., Ojha, T.P., and Upreti, B.N., 1998a, Neogene foreland basin deposits, erosional unroofing, and the kinematic history of the Himalayan fold-thrust belt, western Nepal: Geological Society of America Bulletin, v. 110, p. 2–21, doi:10.1130/0016-7606(1998)110<0002:NFBDEU>2.3.CO;2.

DeCelles, P.G., Gehrels, G.E., Quade, J., and Ojha, T.P., 1998b, Eocene–early Miocene foreland basin development and the history of Himalayan thrusting, western and central Nepal: Tectonics, v. 17, p. 741–765, doi:10.1029/98TC02598.

DeCelles, P.G., Gehrels, G.E., Quade, J., Lareau, B., and Spurlin, M., 2000, Tectonic implications of U-Pb zircon ages of the Himalayan orogenic belt in Nepal: Science, v. 288, p. 497–499, doi:10.1126/science.288.5465.497.

DeCelles, P.G., Robinson, D.M., Quade, J., Copeland, P., Upreti, B.N., Ojha, T.P., and Garzione, C.N., 2001, Regional structure and stratigraphy of the Himalayan fold-thrust belt, far western Nepal: Tectonics, v. 20, p. 487–509, doi:10.1029/2000TC001226.

DeCelles, P.G., Gehrels, G.E., Najman, Y., Martin, A.J., Carter, A., and Garzanti, E., 2004, Detrital geochronology and geochemistry of Cretaceous–early Miocene strata of Nepal: Implications for timing and diachroneity of initial Himalayan orogenesis: Earth and Planetary Science Letters, v. 227, p. 313–330, doi:10.1016/j.epsl.2004.08.019.

DeCelles, P.G., Kapp, P., Ding, L., and Gehrels, G.E., 2007, Late Cretaceous to Middle Tertiary basin evolution in the central Tibetan Plateau: Changing environments in response to tectonic partitioning, aridification, and regional elevation gain: Geological Society of America Bulletin, v. 119, p. 654–680, doi:10.1130/B26074.1.

Ding, L., Kapp, P., and Wan, X., 2005, Paleocene-Eocene record of ophiolite obduction and initial India-Asia collision, south central Tibet: Tectonics, v. 24, TC2001, doi:10.1029/2004TC001729.

Dupont-Nivet, G., Lippert, P., van Hinsbergen, D.J.J., Meijers, M.J.M., and Kapp, P., 2010, Paleolatitude and age of the Indo-Asia collision: Paleomagnetic constraints: Geophysical Journal International, v. 182, p. 1189–1198, doi:10.1111/j.1365-246X.2010.04697.x.

Echavarria, L., Hernández, R., Allmendinger, R., and Reynolds, J., 2003, Subandean thrust and fold belt of northwestern Argentina: Geometry and timing of the Andean evolution: The American Association of Petroleum Geologists Bulletin, v. 87, p. 965–985, doi:10.1306/01200300196.

Fuchs, G.R., and Frank, W., 1970, The geology of west Nepal between the rivers Kali Gandaki and Thulo Bheri: Jahrbuch der Geologischen Bundesanstalt, v. 18, 103 p.

Galy, A., and France-Lanord, C., 2001, Higher erosion rates in the Himalaya: Geochemical constraints on riverine fluxes: Geology, v. 29, p. 23–26, doi:10.1130/0091-7613(2001)029<0023:HERITH>2.0.CO;2.

Gansser, A., 1964, Geology of the Himalayas: London, Wiley Interscience, 289 p.

Gautam, P., and Fujiwara, Y., 2000, Magnetic polarity stratigraphy of Siwalik Group sediments of Karnali River section in western Nepal: Geophysical Journal International, v. 142, p. 812–824, doi:10.1046/j.1365-246x.2000.00185.x.

Gehrels, G.E., DeCelles, P.G., Martin, A., Ojha, T.P., Pinhassi, G., and Upreti, B.N., 2003, Initiation of the Himalayan orogen as an early Paleozoic thin-skinned thrust belt: GSA Today, v. 13, no. 9, p. 4–9, doi:10.1130/1052-5173(2003)13<4:IOTHOA>2.0.CO;2.

Gehrels, G.E., DeCelles, P.G., Ojha, T.P., and Upreti, B.N., 2006, Geologic and U-Th-Pb geochronologic evidence for early Paleozoic tectonism in the Kathmandu thrust sheet, central Nepal Himalaya: Geological Society of America Bulletin, v. 118, p. 185–198, doi:10.1130/B25753.1.

Gehrels, G.E., Kapp, P., DeCelles, P., Pullen, A., Blakey, R., Weislogel, A., Ding, L., Guynn, J., Martin, A., McQuarrie, N., and Yin, A., 2011, Detrital zircon geochronology of pre-Tertiary strata in the Tibetan-Himalayan orogen: Tectonics, v. 30, TC5016, doi:10.1029/2011TC002868.

Green, O.R., Searle, M.P., Corfield, R.I., and Corfield, R.M., 2008, Cretaceous–Tertiary carbonate platform evolution and the age of the India-Asia collision along the Ladakh Himalaya (northwest India): The Journal of Geology, v. 116, p. 331–353, doi:10.1086/588831.

Hames, W.E., and Bowring, S.A., 1994, An empirical evaluation of the argon diffusion geometry in muscovite: Earth and Planetary Science Letters, v. 124, p. 161–169, doi:10.1016/0012-821X(94)00079-4.

Hatcher, R.D., and Hooper, R.J., 1992, Evolution of crystalline thrust sheet in the internal parts of mountain chains, *in* McClay, K.R., ed., Thrust Tectonics: New York, Chapman and Hall, p. 217–233.

Herman, F., Copeland, P., Avouac, J.-P., Bollinger, L., Mahéo, G., LeFort, P., Rai, S., Foster, D., Pêcher, A., Stuwe, K., and Henry, P., 2010, Exhumation, crustal deformation, and thermal structure of the Nepal Himalaya derived from the inversion of thermochronological and thermobarometric data and modeling of the topography: Journal of Geophysical Research, v. 115, B06407, doi:10.1029/2008JB006126.

Hetzel, R., Dunkl, I., Haider, V., Strobl, M., von Eynatten, H., Ding, L., and Frei, D., 2011, Peneplain formation in southern Tibet predates the India-Asia collision and plateau uplift: Geology, v. 39, p. 983–986, doi:10.1130/G32069.1.

Hodges, K.V., 2000, Tectonics of the Himalaya and southern Tibet from two perspectives: Geological Society of America Bulletin, v. 112, p. 324–350, doi: 10.1130/0016-7606(2000)112<0324:TOTHAS>2.3.CO;2.

Hurford, A.J., 1986, Cooling and uplift patterns in the Lepontine Alps, south central Switzerland, and an age of vertical movement on the Insubric fault line: Contributions to Mineralogy and Petrology, v. 92, p. 413–427, doi:10.1007/BF00374424.

Huyghe, P., Galy, A., Mugnier, J.-L., and France-Lanord, C., 2001, Propagation of the thrust system and erosion in the Lesser Himalaya: Geochemical and sedimentological evidence: Geology, v. 29, p. 1007–1010, doi:10.1130/0091-7613(2001)029<1007:POTTSA>2.0.CO;2.

Huyghe, P., Mugnier, J.-L., Gaurel, A.P., and Delcaillau, B., 2005, Tectonic and climatic control of the changes in the sedimentary record of the Karnali River section (Siwaliks of western Nepal): The Island Arc, v. 14, p. 311–327, doi:10.1111/j.1440-1738.2005.00500.x.

Johnson, M.R.W., 2005, Structural settings for the contrary metamorphic zonal sequences in the internal and external zones of the Himalaya: Journal of Asian Earth Sciences, v. 25, p. 695–706, doi:10.1016/j.jseaes.2004.04.010.

Johnson, M.R.W., Oliver, G.J.H., Parrish, R.R., and Johnson, S.P., 2001, Synthrusting metamorphism, cooling, and erosion of the Himalayan Kathmandu Complex, Nepal: Tectonics, v. 20, p. 394–415, doi:10.1029/2001TC900005.

Jordan, T.A., and Watts, A.B., 2005, Gravity anomalies, flexure and the elastic thickness structure of the India-Eurasia collisional system: Earth and Planetary Science Letters, v. 236, p. 732–750, doi:10.1016/j.epsl.2005.05.036.

Kohn, M.J., 2008, *P-T-t* data from central Nepal support critical taper and repudiate large-scale channel flow of the Greater Himalayan sequence: Geological Society of America Bulletin, v. 120, p. 259–273, doi:10.1130/B26252.1.

Kohn, M.J., Wieland, M., Parkinson, C.D., and Upreti, B.N., 2004, Miocene faulting at plate tectonic velocity in the Himalaya of central Nepal: Earth and Planetary Science Letters, v. 228, p. 299–310, doi:10.1016/j.epsl.2004.10.007.

Kohn, M.J., Paul, S.K., and Corrie, S.L., 2010, The lower Lesser Himalayan sequence: A Paleoproterozoic arc on the northern margin of the Indian plate: Geological Society of America Bulletin, v. 122, p. 323–335, doi:10.1130/B26587.1.

Koons, P.O., 1990, Two-sided orogen: Collision and erosion from the sandbox to the Southern Alps, New Zealand: Geology, v. 18, p. 679–682, doi:10.1130/0091-7613(1990)018<0679:TSOCAE>2.3.CO;2.

Larson, K.P., Godin, L., and Price, R.A., 2010, Relationships between displacement and distortion in orogens: Linking the Himalayan foreland and hinterland in central Nepal: Geological Society of America Bulletin, v. 122, p. 1116–1134, doi:10.1130/B30073.1.

Lavé, J., and Avouac, J.P., 2000, Active folding of fluvial terraces across the Siwaliks Hills, Himalayas of central Nepal: Journal of Geophysical Research, v. 105, p. 5735–5770, doi:10.1029/1999JB900292.

Law, R.D., Searle, M.P., and Simpson, R.L., 2004, Strain, deformation temperatures and vorticity of flow at the top of the Greater Himalayan slab, Everest Massif, Tibet: Journal of the Geological Society of London, v. 161, p. 305–320, doi:10.1144/0016-764903-047.

Leech, M.L., Singh, S., Jain, A.K., Klemperer, S.L., and Manickavasagam, R.M., 2005, The onset of India-Asia continental collision: Early, steep subduction required by the timing of UHP metamorphism in the western Himalaya: Earth and Planetary Science Letters, v. 234, p. 83–97, doi:10.1016/j.epsl.2005.02.038.

LeFort, P., 1975, Himalayas: The collided range: Present knowledge of the continental arc: American Journal of Science, v. 275-A, p. 1–44.

LeFort, P., 1986, Metamorphism and magmatism during the Himalayan collision, *in* Coward, M.P., and Ries, A.C., eds., Collision Tectonics: Geological Society of London Special Publication 19, p. 159–172.

Long, S.P., and McQuarrie, N., 2010, Placing limits on channel flow: Insights from the Bhutan Himalaya: Earth and Planetary Science Letters, v. 290, p. 375–390, doi:10.1016/j.epsl.2009.12.033.

Long, S.P., McQuarrie, N., Tobgay, T., and Grujic, D., 2011, Geometry and crustal shortening of the Himalayan fold-thrust belt in Bhutan: Geological Society of America Bulletin, v. 123, p. 1406–1426, doi:10.1130/B30203.1.

Lyon-Caen, H., and Molnar, P., 1985, Gravity anomalies, flexure of the Indian plate, and the structure, support and evolution of the Himalaya and Ganga Basin: Tectonics, v. 4, p. 513–538, doi:10.1029/TC004i006p00513.

Martin, A.J., DeCelles, P.G., Gehrels, P.G., Patchett, P.J., and Isachsen, C., 2005, Isotopic and structural constraints on the location of the Main Central thrust in the Annapurna Range, central Nepal Himalaya: Geological Society of America Bulletin, v. 117, p. 926–944, doi:10.1130/B25646.1.

Martin, A.J., Burgy, K.D., Kaufman, A.J., and Gehrels, G.E., 2011, Stratigraphic and tectonic implications of field and isotopic constraints on depositional ages of Proterozoic Lesser Himalayan rocks in central Nepal: Precambrian Research, v. 185, p. 1–17, doi:10.1016/j.precamres.2010.11.003.

McQuarrie, N., Horton, B.K., Zandt, G., Beck, S., and DeCelles, P.G., 2005, Lithospheric evolution of the Andean fold-thrust belt, Bolivia, and the origin of the central Andean plateau: Tectonophysics, v. 399, p. 15–37.

McQuarrie, N., Barnes, J., and Ehlers, T.A., 2008, Geometric, kinematic and erosional history of the central Andean Plateau (15–17°S), northern Bolivia: Tectonics, v. 27, TC3007, doi:10.1029/2006TC002054.

Mitra, G., 1978, Ductile deformation zones and mylonites: The mechanical processes involved in the deformation of crystalline basement rocks: American Journal of Science, v. 278, p. 1057–1084, doi:10.2475/ajs.278.8.1057.

Murphy, M.A., and Copeland, P., 2005, Transtensional deformation in the central Himalaya and its role in accommodating growth of the Himalayan orogen: Tectonics, v. 24, TC4012, doi:10.1029/2004TC001659.

Murphy, M.A., and Yin, A., 2003, Structural evolution and sequence of thrusting in the Tethyan fold-thrust belt and Indus-Yalu suture zone, southwest Tibet: Geological Society of America Bulletin, v. 115, p. 21–34, doi:10.1130/0016-7606(2003)115<0021:SEASOT>2.0.CO;2.

Myrow, P.M., Hughes, N.C., Paulsen, T.S., Williams, I.S., Parcha, S.K., Thompson, K.R., Bowring, S.A., Peng, S.-C., and Ahluwalia, A.D., 2003, Integrated tectonostratigraphic analysis of the Himalaya and implications for its tectonic reconstruction: Earth and Planetary Science Letters, v. 212, p. 433–441, doi:10.1016/S0012-821X(03)00280-2.

Myrow, P.M., Hughes, N.C., Goodge, J.W., Fanning, C.M., Williams, I.S., Peng, S., Bhargava, O.N., Parcha, S.K., and Pogue, K.R., 2010, Extraordinary transport and mixing of sediment across Himalayan central Gondwana during the Cambrian-Ordovician: Geological Society of America Bulletin, v. 122, p. 1660–1670, doi:10.1130/B30123.1.

Najman, Y., 2006, The detrital record of orogenesis: A review of approaches and techniques used in the Himalayan sedimentary basins: Earth-Science Reviews, v. 72, p. 1–72.

Najman, Y., and Garzanti, E., 2000, Reconstructing early Himalayan tectonic evolution and paleogeography from Tertiary foreland basin sedimentary rocks, northern India: Geological Society of America Bulletin, v. 112, p. 435–449, doi:10.1130/0016-7606(2000)112<435:REHTEA>2.0.CO;2.

Najman, Y.M.R., Pringle, M.S., Johnson, M.W.R., Roberson, A.H.F., and Wijbrans, J.R., 1997, Laser $^{40}Ar/^{39}Ar$ dating of single detrital muscovite grains from early foreland basin deposits in India: Implications for early Himalayan evolution: Geology, v. 25, p. 535–538, doi:10.1130/0091-7613(1997)025<0535:LAADOS>2.3.CO;2.

Najman, Y., Johnson, C., White, N.M., and Oliver, G., 2004, Constraints on foreland basin and orogenic evolution from detrital mineral fission track analyses and sediment facies of the Himalayan foreland basin, NW India: Basin Research, v. 16, p. 1–24, doi:10.1111/j.1365-2117.2004.00223.x.

Najman, Y., Carter, A., Oliver, G., and Garzanti, E., 2005, Provenance of Eocene foreland basin sediments, Nepal: Constraints to the timing and diachroneity of early Himalayan orogenesis: Geology, v. 33, p. 309–312, doi:10.1130/G21161.1.

Najman, Y., Bickle, M., Garzanti, E., Pringle, M., Barfod, D., Brozovic, N., Burbank, D., and Ando, S., 2009, Reconstructing the exhumation history of the Lesser Himalaya, NW India, from a multitechnique provenance study of the foreland basin Siwalik Group: Tectonics, v. 28, TC5018, doi:10.1029/2009TC002506.

Najman, Y., Appel, E., Boudagher-Fadel, M., Bown, P., Carter, A., Garzanti, E., Godin, L., Han, J., Liebke, U., Oliver, G., Parrish, R., and Vezzoli, G., 2010, Timing of India-Asia collision: Geological, biostratigraphic, and palaeomagnetic constraints: Journal of Geophysical Research, v. 115, B12416, doi:10.1029/2010JB007673.

Nakayama, K., and Ulak, P., 1999, Evolution of fluvial style in the Siwalik Group in the foothills of the Nepal Himalaya: Sedimentary Geology, v. 125, p. 205–224, doi:10.1016/S0037-0738(99)00012-3.

Ni, J., and Barazangi, M., 1984, Seismotectonics of the Himalayan collision zone: Geometry of the underthrusting Indian plate beneath the Himalaya: Journal of Geophysical Research, v. 89, p. 1147–1163, doi:10.1029/JB089iB02p01147.

Northrup, C.J., 1996, Structural expressions and tectonic implications of general noncoaxial flow in the midcrust of a collisional orogen: The northern Scandinavian Caledonides: Tectonics, v. 15, p. 490–505, doi:10.1029/95TC02951.

Ojha, T.P., Butler, R.F., Quade, J., DeCelles, P.G., Richards, D., and Upreti, B.N., 2000, Magnetic polarity stratigraphy of the Neogene Siwalik Group at Khutia Khola, far western Nepal: Geological Society of America Bulletin, v. 112, p. 424–434, doi:10.1130/0016-7606(2000)112<424:MPSOTN>2.0.CO;2.

Ojha, T.P., Butler, R.F., DeCelles, P.G., and Quade, J., 2009, Magnetic polarity stratigraphy of the Neogene foreland basin deposits of Nepal: Basin Research, v. 21, p. 61–90, doi:10.1111/j.1365-2117.2008.00374x.

Oncken, O., Hindle, D., Kley, J., Elger, K., Victor, P., and Schemmann, K., 2006, Deformation of the Central Andean upper plate system: Facts, fiction, and constraints for plateau models, *in* Oncken, O., Chong, G., Franz, G., Giese, P., Götze, H.-J., Ramos, V.A., Strecker, M.R., and Wigger, P., eds., The Andes. Active Subduction Orogeny: Frontiers in Earth Sciences Series: Berlin, Springer-Verlag, p. 3–27.

Pandey, M.R., Tandukar, R.P., Avouac, J.P., Vergne, J., and Héritier, T., 1999, Seismotectonics of the Nepal Himalaya from a local seismic network: Journal of Asian Earth Sciences, v. 17, p. 703–712, doi:10.1016/S1367-9120(99)00034-6.

Parrish, R.R., and Hodges, K.V., 1996, Isotopic constraints on the age and provenance of the Lesser and Greater Himalayan sequences, Nepalese Himalaya: Geological Society of America Bulletin, v. 108, p. 904–911, doi:10.1130/0016-7606(1996)108<0904:ICOTAA>2.3.CO;2.

Passchier, C.W., and Trouw, R.A.J., 1996, Micro-Tectonics: Berlin, Springer-Verlag, 289 p.

Patel, R.C., Singh, S., Asokan, A., Manickavasagam, R.M., and Jain, A.K., 1993, Extensional tectonics in the Himalayan orogen, Zanskar, *in* Treloar, P.J., and Searle, M.P., eds., Himalayan Tectonics: Geological Society of London Special Publication 74, p. 445–459.

Pearson, O.N., and DeCelles, P.G., 2005, Structural geology and regional tectonic significance of the Ramgarh thrust, Himalayan fold-thrust belt of Nepal: Tectonics, v. 24, TC4008, doi:10.1029/2003TC001617.

Quade, J., Cater, J.M.L., Ojha, T.P., Adam, J., and Harrison, T.M., 1995, Late Miocene environmental change in Nepal and the northern Indian subcontinent: Stable isotopic evidence from paleosols: Geological Society of America Bulletin, v. 107, p. 1381–1397, doi:10.1130/0016-7606(1995)107<1381:LMECIN>2.3.CO;2.

Quade, J., Roe, L., DeCelles, P.G., and Ojha, T.P., 1997, The late Neogene $^{87}Sr/^{86}Sr$ record of lowland Himalayan rivers: Science, v. 276, p. 1828–1831, doi:10.1126/science.276.5320.1828.

Rahl, J.M., Haines, S.H., and van der Pluijm, B.A., 2011, Links between orogenic wedge deformation and erosional exhumation: Evidence from illite age analysis of fault rock and detrital thermochronology of syn-tectonic conglomerates in the Spanish Pyrenees: Earth and Planetary Science Letters, v. 307, p. 180–190, doi:10.1016/j.epsl.2011.04.036.

Ratschbacher, L., Frisch, W., and Guanghua, L., 1994, Distributed deformation in southern and western Tibet during and after the India-Asia collision: Journal of Geophysical Research, v. 99, p. 19,917–19,945, doi:10.1029/94JB00932.

Ravikant, V., Wu, F.-Y., and Ji, W.-Q., 2011, U-Pb age and Hf isotopic constraints of detrital zircons from the Himalayan foreland Subathu sub-basin on the Tertiary palaeogeography of the Himalaya: Earth and Planetary Science Letters, v. 304, p. 356–368, doi:10.1016/j.epsl.2011.02.009.

Robert, X., van der Beek, P., Braun, J., Perry, C., Dubille, M., and Mugnier, J.-L., 2009, Assessing Quaternary reactivation of the Main Central thrust zone (central Nepal Himalaya): New thermochronologic data and numerical modeling: Geology, v. 37, p. 731–734, doi:10.1130/G25736A.1.

Robinson, D.M., 2008, Forward modeling the kinematic sequence of the central Himalayan thrust belt, western Nepal: Geosphere, v. 4, p. 785–801, doi:10.1130/GES00163.1.

Robinson, D.M., and Pearson, O.N., 2006, Exhumation of Greater Himalayan rock along the Main Central thrust, Nepal: Implications for channel flow, *in* Law, R.D., Searle, M.P., and Godin, L., eds., Channel Flow, Extrusion, and Exhumation in Continental Collision Zones: Geological Society of London Special Publication 268, p. 255–268.

Robinson, D.M., DeCelles, P.G., Patchett, P.J., and Garzione, C.N., 2001, The kinematic history of the Nepalese Himalaya interpreted from Nd isotopes: Earth and Planetary Science Letters, v. 192, p. 507–521, doi:10.1016/S0012-821X(01)00451-4.

Robinson, D.M., DeCelles, P.G., Garzione, C.N., Pearson, O.N., Harrison, T.M., and Catlos, E.J., 2003, Kinematic model for the Main Central thrust in Nepal: Geology, v. 31, p. 359–362, doi:10.1130/0091-7613(2003)031<0359:KMFTMC>2.0.CO;2.

Robinson, D.M., DeCelles, P.G., and Copeland, P., 2006, Tectonic evolution of the Himalayan thrust belt in western Nepal: Implications for channel flow models: Geological Society of America Bulletin, v. 118, p. 865–885, doi:10.1130/B25911.1.

Rohrmann, A., Kapp, P., Carrapa, B., Reiners, P.W., Guynn, J., Ding, L., and Heizler, M., 2012, Thermochronologic evidence for plateau formation in central Tibet by 45 Ma: Geology, v. 40, p. 187–190, doi:10.1130/G32530.1.

Sakai, H., 1983, Geology of the Tansen Group of the Lesser Himalaya in Nepal: Memoirs of the Faculty of Science: Kyushu University [D], v. 25, p. 27–74.

Sakai, H., 1989, Rifting of the Gondwanaland and uplifting of the Himalayas recorded in Mesozoic and Tertiary fluvial sediments in the Nepal Himalaya, *in* Taira, A., and Masuda, F., eds., Sedimentary Facies in the Active Plate Margin: Tokyo, Japan, Terra Science, p. 723–732.

Sakai, H., Takigami, Y., Nakamuta, Y., and Nomura, H., 1999, Inverted metamorphism in the pre–Siwalik foreland basin sediments beneath the crystalline nappe, western Nepal Himalaya: Journal of Asian Earth Sciences, v. 17, p. 727–739, doi:10.1016/S1367-9120(99)00035-8.

Schelling, D., and Arita, K., 1991, Thrust tectonics, crustal shortening, and the structure of the far-eastern Nepal Himalaya: Tectonics, v. 10, p. 851–862, doi:10.1029/91TC01011.

Searle, M.P., Law, R.D., Godin, L., Larson, K.P., Streule, M.M., Cottle, J.M., and Jessup, M.J., 2008, Defining the Himalayan Main Central thrust in Nepal: Journal of the Geological Society of London, v. 165, p. 523–534, doi:10.1144/0016-76492007-081.

Sinclair, H.D., Gibson, M., Naylor, M., and Morris, R.G., 2005, Asymmetric growth of the Pyrenees revealed through measurement and modeling of orogenic fluxes: American Journal of Science, v. 305, p. 369–406, doi:10.2475/ajs.305.5.369.

Szulc, A.G., Najman, Y., Sinclair, H.D., Pringle, M., Bickle, M., Chapman, H., Garzanti, E., Ando, S., Huyghe, P., Mugnier, J.-L., Ojha, T., and DeCelles, P., 2006, Tectonic evolution of the Himalaya constrained by detrital ^{40}Ar-^{39}Ar, Sm-Nd and petrographic data from the Siwalik foreland basin succession, SW Nepal: Basin Research, v. 18, p. 375–391, doi:10.1111/j.1365-2117.2006.00307.x.

Thiede, R.C., Bookhagen, B., Arrowsmith, J.R., Sobel, E.R., and Strecker, M.R., 2004, Climatic control on rapid exhumation along the southern Himalayan Front: Earth and Planetary Science Letters, v. 222, p. 791–806, doi:10.1016/j.epsl.2004.03.015.

Thiede, R.C., Ehlers, T.A., Bookhagen, B., and Strecker, M.R., 2009, Erosional variability along the northwest Himalaya: Journal of Geophysical Research, v. 114, F01015, doi:10.1029/2008JF001010.

Turcotte, D., and Schubert, G., 1982, Geodynamics: New York, John Wiley, 450 p.

Upreti, B.N., 1996, Stratigraphy of the western Nepal Lesser Himalaya: A synthesis: Journal of Nepal Geological Society, v. 13, p. 11–28.

Upreti, B.N., 1999, An overview of the stratigraphy and tectonics of the Nepal Himalaya: Journal of Asian Earth Sciences, v. 17, p. 577–606, doi:10.1016/S1367-9120(99)00047-4.

Upton, P., Mueller, K., and Chen, Y.-G., 2009, Three-dimensional numerical models with varied material properties and erosion rates: Implications for the mechanics and kinematics of compressive wedges: Journal of Geophysical Research, v. 114, B04408, doi:10.1029/2008JB005708.

van der Beek, P., Robert, X., Mugnier, J.-L., Bernet, M., Huyghe, P., and Labrin, E., 2006, Late-Miocene–Recent exhumation of the central Himalaya and recycling in the foreland basin assessed by apatite fission-track thermochronology of Siwalik sediments, Nepal: Basin Research, v. 18, p. 413–434, doi:10.1111/j.1365-2117.2006.00305.x.

Vannay, J.-C., and Hodges, K.V., 1996, Tectonometamorphic evolution of the Himalayan metamorphic core between the Annapurna and Dhaulagiri, central Nepal: Journal of Metamorphic Geology, v. 14, p. 635–656, doi:10.1046/j.1525-1314.1996.00426.x.

Wang, J., Hu, X., Jansa, L.F., and Huang, Z., 2011, Provenance of the Upper Cretaceous–Eocene deep-water sandstones in Sangdanlin, southern Tibet: Constraints on the timing of initial India-Asia collision: The Journal of Geology, v. 119, p. 293–309, doi:10.1086/659145.

Webb, A.A.G., Yin, A., Harrison, T.M., Célérier, J., Gehrels, G.E., Manning, C.E., and Grove, M., 2011, Cenozoic tectonic history of the Himachal Himalaya (northwestern India) and its constraints on the formation mechanism of the Himalayan orogen: Geosphere, v. 7, p. 1013–1061, doi:10.1130/GES00627.1.

Whipp, D.M., Ehlers, T.A., Blythe, A., Huntington, K., Hodges, K., and Burbank, D.W., 2007, Plio-Quaternary exhumation history of the central Nepalese Himalaya: 2. Thermokinematic and thermochronometer age prediction model: Tectonics, v. 26, TC3003, doi:10.1029/2006TC001991.

Willett, S.D., Beaumont, C., and Fullsack, P., 1993, Mechanical model for the tectonics of doubly vergent orogens: Geology, v. 21, p. 371–174, doi:10.1130/0091-7613(1993)021<0371:MMFTTO>2.3.CO;2.

Wobus, C.W., Hodges, K.V., and Whipple, K.X., 2003, Has focused denudation sustained active thrusting at the Himalayan topographic front?: Geology, v. 31, p. 861–864, doi:10.1130/G19730.1.

Zhang, J., and Guo, L., 2007, Structure and geochronology of the southern Xainza-Dinggye rift and its relationship to the South Tibetan detachment system: Journal of Asian Earth Sciences, v. 29, p. 722–736, doi:10.1016/j.jseaes.2006.05.003.

Zhu, B., Kidd, W.S.F., Rowley, D.B., Currie, B.S., and Shafique, N., 2005, Age of initiation of the India-Asia collision in the east-central Himalaya: The Journal of Geology, v. 113, p. 265–285, doi:10.1086/428805.

MANUSCRIPT RECEIVED 31 JANUARY 2012
REVISED MANUSCRIPT RECEIVED 28 JUNE 2012
MANUSCRIPT ACCEPTED 2 JULY 2012

Printed in the USA

Statement of Ownership, Management, and Circulation

(Required by Title 39 U.S.C. 4369)

Lithosphere (Publication No. 1941-8264) is published bi-monthly by The Geological Society of America, Inc., (GSA) with headquarters and offices at 3300 Penrose Place, Boulder, Colorado 80301 U.S.A.; and mailing address of Post Office Box 9140, Boulder, Colorado 80301-9140 U.S.A. The Publisher is Jon Olsen; the Managing Editor is Bryan Hibbard; their offices and mailing addresses are the same as above. The annual subscription prices are: GSA Members $60; GSA Student/K-12 Teacher Members $35; non-members $450. The publication is wholly owned by The Geological Society of America, Inc., a not-for-profit, charitable corporation. No known stockholder holds 1 percent or more of the total stock. There are no known mortgagees or holders of other securities. The purpose, function, and nonprofit status of The Geological Society of America, Inc., has not changed during the preceding twelve months. The average number of copies of each issue during the preceding twelve months and the actual number of copies published nearest to the filing date (August 2012 issue) are noted at right.

This information taken from PS Form 3526, signed 17 September 2012 by the Publisher, Jon Olsen, and filed with the United States Postal Service in Boulder, Colorado.

Item No. from PS Form 3526	Avg. No. Copies Each Issue in Past 12 Months	Actual No. Copies of Single Issue Published Nearest to Filing Date
15. Extent and Nature of Circulation		
a. Total number of copies (*net press run*)	425	450
b. Legitimate paid and/or requested distribution (*by mail and outside the mail*)	296	318
c. Total paid and/or requested circulation	296	318
d. Nonrequested distribution (*by mail and outside the mail*)	0	0
e. Total nonrequested distribution	0	0
f. Total distribution (*sum of c and e*)	296	318
g. Copies not distributed (*office use, leftovers, spoiled*)	129	132
h. Total (*sum of f and g*)	425	450
i. Percent paid and/or requested circulation (c/f × 100)	100%	100%